Small molecule antagonist reveals seizure-induced mediation of neuronal injury by prostaglandin E2 receptor subtype EP2

Jianxiong Jiang[a,1,2], Thota Ganesh[a,b,1], Yuhong Du[a,b,1], Yi Quan[a], Geidy Serrano[a], Min Qui[a,b], Iris Speigel[a], Asheebo Rojas[a], Nadia Lelutiu[a], and Raymond Dingledine[a,b,2]

[a]Department of Pharmacology, [b]Emory Chemical Biology Discovery Center, Emory University School of Medicine, Atlanta, GA 30322

Edited by Solomon H. Snyder, Johns Hopkins University School of Medicine, Baltimore, MD, and approved January 17, 2012 (received for review December 8, 2011)

With interest waning in the use of cyclooxygenase-2 (COX-2) inhibitors for inflammatory disease, prostaglandin receptors provide alternative targets for the treatment of COX-2–mediated pathological conditions in both the periphery and the central nervous system. Activation of prostaglandin E2 receptor (PGE_2) subtype EP2 promotes inflammation and is just beginning to be explored as a therapeutic target. To better understand physiological and pathological functions of the prostaglandin EP2 receptor, we developed a suite of small molecules with a 3-aryl-acrylamide scaffold as selective EP2 antagonists. The 12 most potent compounds displayed competitive antagonism of the human EP2 receptor with K_B 2–20 nM in Schild regression analysis and 268- to 4,730-fold selectivity over the prostaglandin EP4 receptor. A brain-permeant compound completely suppressed the up-regulation of COX-2 mRNA in rat cultured microglia by EP2 activation and significantly reduced neuronal injury in hippocampus when administered in mice beginning 1 h after termination of pilocarpine-induced status epilepticus. The salutary actions of this novel group of antagonists raise the possibility that selective block of EP2 signaling via small molecules can be an innovative therapeutic strategy for inflammation-related brain injury.

cAMP | brain inflammation | neurodegeneration | neuroprotection | epilepsy

Cyclooxygenase-2 (COX-2), the inducible isoform of COX, is rapidly up-regulated in damaged tissue, for example in the central nervous system (CNS) after a seizure or cerebral ischemia (1–3). COX-2 induction in CNS overall contributes to inflammation and injury mainly by producing prostanoids (4–7). However, the deleterious cardio- and cerebrovascular side effects from sustained inhibition of COX-2 suggest that some COX-2 downstream prostanoid signaling might be beneficial (8), such that modulation of a specific prostanoid receptor or synthase could be a superior therapeutic strategy compared with generic block of the entire COX-2 cascade. Prostaglandin E2 (PGE_2), a dominant enzymatic product of COX-2 in the brain, can activate four G-protein–coupled receptors (GPCRs): EP1, EP2, EP3, and EP4. Among these, EP2 and EP4 receptors are positively coupled through Gαs to cAMP production (9). In turn, cAMP can initiate multiple downstream events mediated by protein kinase A (PKA) or exchange protein activated by cAMP (Epac) (9).

The EP2 receptor is widely expressed in both neurons and glia (3, 10). Neuronal EP2 activation appears to mediate some beneficial effects, such as PKA-dependent neuroprotection in acute models of ischemia and excitotoxicity (3, 11, 12), early neuroprotection following seizures (13), and promotion of spatial learning (14). Conversely, on the basis of the phenotype of EP2 knockout mice, EP2 activation is thought to promote inflammation and neurotoxicity in animal models of neurodegenerative diseases including Alzheimer's disease (15), Parkinson's disease (16), and amyotrophic lateral sclerosis (10). Glial, especially microglial EP2, is considered to play a major role in brain inflammation associated with chronic neurologic disorders (10, 16). Genetic ablation of the EP2 receptor reduces oxidative stress and improves cell survival, accompanied by substantial down-regulation of enzymes that produce reactive oxygen or nitrogen species such as inducible nitric oxide synthase (iNOS), NADPH oxidase (NOX), and COX-2 itself (10). EP2 receptor activation by PGE_2 has also been reported to elevate iNOS expression in activated astrocytes by potentiating the response to the inflammatory cytokines TNF-α and IFN-γ (17). Moreover, the EP2 receptor is involved in spinal inflammatory hyperalgesia and neuropathic pain (18, 19). In the past 2 decades inflammation has emerged as a common feature in many if not all chronic neurological disorders and is widely believed to play a pivotal role in subsequent neuropathogenesis (20). For these reasons we hypothesized that pharmacologic block of PGE_2/EP2 signaling might represent an innovative strategy to mitigate inflammation and protect neuronal tissue in neurological disorders.

All previous conclusions on the roles of PGE_2/EP2 signaling were made on the basis of studies using either a selective EP2 agonist (e.g., butaprost) or mice deficient in the EP2 gene. Parallel data from direct pharmacological inhibition of EP2 receptors are missing, because in contrast to all other prostaglandin receptors no selective antagonists for the EP2 receptor have been reported until recently (21). We developed a set of cell-based time-resolved fluorescence resonance energy transfer (TR-FRET) assays of cAMP formation that are suitable for high-throughput screening (HTS) and we used these assays to discover and then chemically modify novel selective competitive antagonists of this key prostaglandin receptor. Here, we report that a series of small molecules sharing a 3-aryl-acrylamide scaffold show high potency and good selectivity for inhibiting PGE_2-induced cAMP accumulation in both human and mouse EP2-expressing cells and have sufficient pharmacokinetic properties to be useful in vivo. These small molecules completely suppressed the EP2–up-regulated inflammatory mediator COX-2 in rat primary microglial cultures. Administration of an EP2 antagonist in mice after pilocarpine-induced status epilepticus (SE) significantly reduced neurodegeneration in hippocampus. These results reinforce the value of the prostaglandin EP2 receptor as a potential neuroprotection target in epilepsy and other inflammation-related neurological disorders. This work was reported in preliminary form (22, 23).

Author contributions: J.J. and R.D. designed research; J.J., T.G., Y.D., Y.Q., and R.D. performed research; G.S., M.Q., I.S., A.R., and N.L. contributed new reagents/analytic tools; J.J. and R.D. analyzed data; and J.J. and R.D. wrote the paper.

The authors declare no conflict of interest.

This article is a PNAS Direct Submission.

Accession: The screening data reported in this paper have been deposited in the PubChem database, http://pubchem.ncbi.nlm.nih.gov (assay ID no. 1422).

[1]J.J., T.G., and Y.D. contributed equally to this work.

[2]To whom correspondence may be addressed. E-mail: rdingledine@pharm.emory.edu or jjiang3@emory.edu.

This article contains supporting information online at www.pnas.org/lookup/suppl/doi:10.1073/pnas.1120195109/-/DCSupplemental.

Results

Potent and Selective Antagonists for Human EP2 Receptors. Using a set of cell-based TR-FRET assays of cAMP formation, we screened a library of 262,371 small molecules and identified a series of compounds as antagonists of human prostaglandin EP2 receptor (Figs. S1 and S2). Among those, hits PubChem substance identification number (SID) 17,515,129 (resynthesized as TG4-155) and SID 17,515,102 (TG4-166) are the most potent ones (Fig. 1*A*) and showed robust inhibition of PGE_2 (1 μM)-induced cAMP accumulation (i.e., reduction of the TR-FRET signal) in human EP2-overexpressing C6 glioma (C6G-EP2) cells (11), without affecting prostaglandin EP4 or β2-adrenergic receptors under agonist-saturated conditions (*SI Results* and Fig. S1). The potency of compounds was further evaluated by their effects on the dose–response curves of PGE_2 and butaprost, the EP2 selective agonist, in C6G-EP2 cells. Cells were incubated first with vehicle or a fixed concentration (1 μM) of test compound for 5 min and then with increasing concentrations of PGE_2 or butaprost for 40 min to induce cAMP accumulation. Both compounds caused a robust rightward shift in the PGE_2 dose–response curve without affecting the maximal response to PGE_2. TG4-155 (1 μM) caused 1,120-fold shift and TG4-166 (1 μM) caused a 651-fold shift in the PGE_2 EC_{50} (Fig. 1*B*). TG4-155 and TG4-166 also caused robust inhibition of the EP2 response to butaprost in C6G-EP2 cells, TG4-155 (1 μM) producing a 962-fold rightward shift and TG4-166 (1 μM) a 678-fold shift in the butaprost EC_{50} (Fig. 1*C*). The quantitatively similar extent of inhibition by TG4-155 and TG4-166 against EP2 receptor activation by PGE_2 or butaprost demonstrates that EP2 inhibition is not agonist specific.

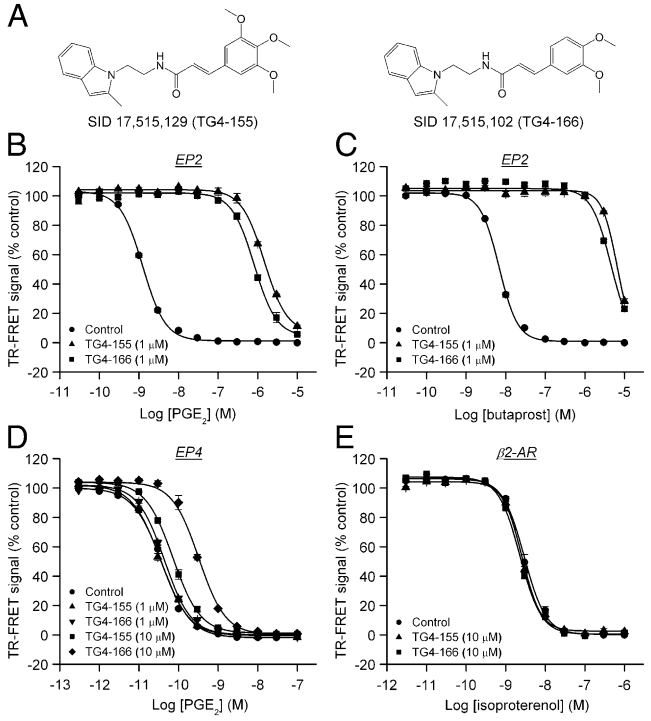

Fig. 1. Selective inhibition of EP2 receptor by hit compounds. (*A*) Chemical structures of TG4-155 and TG4-166. (*B*) TG4-155 and TG4-166 caused rightward shifts in the PGE_2 dose–response curves in C6G-EP2 cells. TG4-155 (1 μM) caused a 1,120-fold shift and TG4-166 (1 μM) caused a 651-fold shift in the PGE_2 EC_{50}. (*C*) TG4-155 (1 μM) caused a 962-fold shift and TG4-166 (1 μM) caused a 678-fold shift in the butaprost EC_{50} in C6G-EP2 cells. (*D*) TG4-155 and TG4-166 (1 μM) had no effect on prostaglandin EP4 receptor. At 10 μM, TG4-155 caused only a 1.8-fold shift and TG4-166 caused an 8.6-fold shift in the PGE_2 EC_{50} in HEK-EP4 cells. (*E*) There was no effect of TG4-155 and TG4-166 (10 μM) on β2-adrenergic receptor as shown by overlapping isoproterenol dose–response curves. Data were normalized as percentage of maximum response; points represent mean ± SEM (n = 4).

We next determined the functional selectivity of these hits for inhibiting EP2 receptors relative to other Gαs-coupled GPCRs. Cells expressing human EP4 or β2-adrenergic receptor were incubated with vehicle, 1 or 10 μM test compound and subsequently stimulated with increasing concentrations of PGE_2 or isoproterenol, respectively. TG4-155 and TG4-166 at 1 μM had no effect on prostaglandin EP4 receptors as shown by virtually overlapping PGE_2 dose–response curves (Fig. 1*D*). Even at 10 μM, TG4-155 caused <2-fold shift and TG4-166 caused <10-fold shift in the PGE_2 EC_{50} in HEK-EP4 cells (Fig. 1*D*). There was also no effect of TG4-155 and TG4-166 (10 μM) on β2-adrenergic receptors as shown by overlapping isoproterenol dose–response curves (Fig. 1*E*). Both EP4 and β2-adrenergic receptors are Gαs-coupled GPCRs, and EP4 is also activated by PGE_2. Therefore, these results suggest that the compounds are selective for the EP2 receptor over EP4 and β2-adrenergic receptors. The selectivity of TG4-155 was further tested in cell-based functional assays against a panel of other GPCRs in leukotriene and prostanoid receptor families. TG4-155 displayed at least 500-fold selectivity for the human EP2 receptor over human BLT1, EP1, EP3, and FP receptors; 345-fold selectivity against human TP receptor; 240-fold selectivity against human IP receptor; and 7-fold selectivity against human DP1 receptor (Fig. S3). In addition, TG4-155 did not show substantial inhibition of COX-1 and COX-2 at 10 μM (Fig. S3). These results indicate that of the nine canonical prostanoid receptors, TG4-155 shows nanomolar antagonist activity against only EP2 and DP1.

EP2 Antagonism Is Competitive. Information on mechanisms of inhibition can be obtained by performing a Schild regression analysis characterized by the equation $\log(dr - 1) = \log X_B - \log K_B$, where dose ratio (dr) is the fold shift in EC_{50}, X_B is [antagonist], and K_B is the equilibrium dissociation constant for the antagonist–receptor complex. A linear regression of log(dr − 1) on log X_B with a slope of unity characterizes a competitive antagonism and the K_B value indicates the antagonist concentration required for a twofold rightward shift in the dose–response curve. Thus, a lower K_B value indicates a higher inhibitory potency. To perform the Schild regression, C6G-EP2 cells were incubated first with vehicle, 0.01, 0.1, or 1 μM of test compound for 5 min and then with increasing concentrations of PGE_2 for 40 min to activate EP2 receptors. All compounds induced concentration-dependent, parallel rightward shifts in the PGE_2 dose–response curve (Fig. 2 *A*–*C*). The Schild regression analyses demonstrated that these compounds have a competitive mechanism of antagonism of EP2 receptor as illustrated by TG4-155 and TG4-166 with K_B = 2.4 nM and K_B = 4.6 nM, respectively (Fig. 2*D* and Table 1). TG4-155 displayed a high affinity to human EP2 receptors with K_i = 15 nM in the radioligand binding assay (Fig. S3). The Schild regression analyses also revealed selectivity for EP2 over EP4 because the K_B for antagonism of EP4 was 4,730-fold (TG4-155) and 435-fold (TG4-166) higher than for EP2 (Table 1 and Fig. 2 *E* and *F*).

Structure–Activity Relationships. To obtain information on structure–activity relationships (SAR), we synthesized 27 small molecules based on the 3-aryl-acrylamide scaffold in TG4-155, (E)-*N*-(2-(2-methyl-1H-indol-1-yl)ethyl)-3-(3,4,5-trimethoxyphenyl) acrylamide, and TG4-166, (E)-3-(3,4-dimethoxyphenyl)-*N*-(2-(2-methyl-1H-indol-1-yl)ethyl)acrylamide (Fig. S4). Four moieties were examined as determinants of compound potency and selectivity: methylindol, ethyl linker, acrylamide, and methoxyphenyl (Fig. 3). All compounds were evaluated for inhibitory potency on EP2 and EP4 receptors by measuring the Schild K_B values. Overall, compounds with a methylindol or fluoro-methylindol ring, ethyl linker, acrylamide, and methoxyphenyl or halogenphenyl retain activities in the low nanomolar range (*SI Results*, Fig. 3, and Table 1). Introduction of fluorine (e.g., TG4-290–1 and

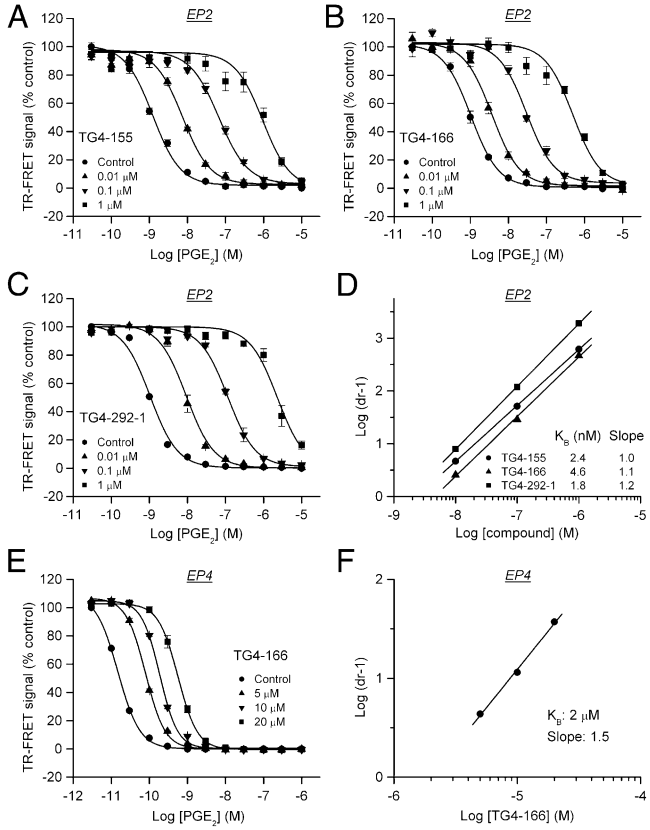

Fig. 2. Competitive antagonism of EP2 receptor. (*A*–*C*) Hits TG4-155, TG4-166, and analog TG4-292-1 inhibited PGE_2-induced human EP2 receptor activation in a concentration-dependent manner. (*D*) Schild regression analysis was performed to elucidate the modality of antagonism from these compounds. TG4-155, TG4-166, and TG4-292-1 displayed a competitive antagonism mode of action on EP2 receptor shown by Schild plots. K_B = 2.4, 4.6, and 1.8 nM; slopes, 1.0, 1.1, and 1.2 for TG4-155, TG4-166, and TG4-292-1, respectively. (*E*) EP2 antagonist compounds showed low potency on human EP4 receptor in HEK-EP4 cells, as illustrated by TG4-166. (*F*) Schild regression analysis was performed to evaluate inhibition of human EP4 receptor by TG4-166. K_B = 2 μM; slope, 1.5. Data were normalized as percentage of maximum response; points represent mean ± SEM (n = 4).

TG6-10–1 in the western side and TG6-94–2 in the eastern side) to improve compound pharmacokinetic properties increased the in vitro metabolic stability of compounds, measured in mouse or human liver microsomes (*SI Results*, Fig. 3, and Fig. S5). All test compounds showed no significant cytotoxicity by measuring the half-maximal cytotoxic concentrations (CC_{50}) in C6G cells (Table 1), as illustrated by TG4-155 and TG4-166 in Fig. S6. Compared with hits TG4-155 and TG4-166, analogs TG4-290-1, TG4-292-1, and TG4-294-2 displayed improved potencies for EP2 receptor inhibition with K_B = 2.1 nM, 1.8 nM, and 1.9 nM; in vitro therapeutic indexes (CC_{50}/K_B for EP2) of 73,800, 387,000, and 253,000; and selectivity indexes (K_B for EP4/K_B for EP2) of 2,600, 1,200, and 2,470 (Fig. 2 and Table 1).

Microglial EP2 Activation Induces COX-2. Microglia are regarded as the resident macrophages in the CNS and thus believed to play a pivotal role in inflammation-mediated neurodegeneration in various models of neurological disorders (24). COX-2 is well recognized as a major mediator of inflammation and neurotoxicity (7), and following seizures COX-2 up-regulation in neurons triggers an inflammatory reaction in the brain (13). The activation of EP2 receptors on microglia, presumably by PGE_2 produced from neuronal COX-2, has been proposed to play an important role in brain inflammation (10, 16). To examine the

Table 1. Activity, cytotoxicity, and selectivity for EP2 antagonist compounds

Analog no.	*K_B EP2, nM	†CC_{50}, μM	‡Therapeutic index	§K_B EP4, μM	¶Selectivity index
TG4-155	2.4	172	71,700	11.4	4,730
TG4-166	4.6	397	86,300	2.0	435
TG4-211-1	348	360	1,030	13.7	39
TG4-211-2	947	448	473	13.3	14
TG4-215-2	1,490	325	219	15.3	10
TG4-161	2,520	311	123	13.9	6
TG6-109-1	Inactive	316	NA	18.9	NA
TG4-290-1	2.1	155	73,800	5.4	2,600
TG4-290-2	22.2	264	11,900	1.7	77
TG6-10-1	21.4	81	3,790	13.4	626
TG6-10-2	58.8	209	3,550	22.4	381
TG4-154	1,860	182	98	5.7	3
TG6-78	185	278	1,500	16.6	90
TG4-156	214	397	1,860	18.1	85
TG6-94-1	16.5	3,090	187,000	8.0	484
TG6-97-1	42.4	653	15,400	11.7	277
TG4-215-1	18.1	146	8,070	11.4	629
TG4-292-2	7.2	517	71,800	1.9	268
TG6-109-2	82.4	199	2,420	30.2	367
TG6-94-2	3.8	89	23,400	10.6	2,800
TG6-97-2	7.0	684	97,700	13.9	1,990
TG6-94-3	18.7	46	2,460	17.2	921
TG6-97-3	27.8	62	2,230	19.9	715
TG4-292-1	1.8	696	387,000	2.2	1,200
TG4-294-1	6.3	601	95,400	3.3	525
TG4-294-2	1.9	481	253,000	4.7	2,470
TG6-110	8.0	1,240	155,000	6.9	859

NA: not applicable.
*K_B (nM) value for EP2 receptor from Schild regression analysis.
†Half-maximal cytotoxic concentration (CC_{50}) in C6G cells after 48 h incubation.
‡In vitro therapeutic index determined by CC_{50}/K_B for EP2.
§K_B (μM) value for EP4 receptor from Schild regression analysis.
¶Selectivity index, determined by K_B EP4/K_B EP2.

activity of TG4-155 on native EP2 receptors, rat primary microglial cultures were preincubated with vehicle or increasing concentrations of TG4-155 for 30 min, followed by addition of butaprost in the presence of antagonist for 2 h. The cellular cAMP levels were evaluated by TR-FRET assay and the induction of COX-2 mRNA was measured by quantitative real-time PCR (qRT-PCR). Butaprost induced a substantial increase of cAMP level in rat primary microglia with an EC_{50} value of 0.5 μM, and TG4-155 displayed robust competitive inhibition of butaprost-induced EP2 activation in a concentration-dependent manner with potency equivalent to a Schild K_B of 5 nM (Fig. 4*A*).

EP2 receptor activation on microglia causes induction of proinflammatory cytokines and other mediators (25). We studied EP2-mediated induction of COX-2 because induction is rapid and large in comparison with other inflammatory mediators. EP2 activation by 1 μM butaprost for 2 h did not affect expression of the EP2 receptor itself in microglia (Fig. 4*B*), but increased COX-2 expression 16.3-fold (Fig. 4*C*). The up-regulation of COX-2 by microglial EP2 was returned to the basal level by 100 nM TG4-155, but not below basal (Fig. 4*B*). It is unlikely that the DP1 receptor is involved in this inhibitory effect on COX-2 induction for the following reasons. First, 1 μM butaprost does not activate DP1 (26); second, TG4-155 inhibits DP1 by <50% at 100 nM (Fig. S3); third, the DP1 agonist, BW245C (26), does not induce COX-2 mRNA at a concentration selective for DP1 under the same conditions (Fig. 4*D*); finally, a 2-h assay incubation would be insufficient time to produce significant COX-2 protein (if indeed the mRNA is translated in microglia) and hence the

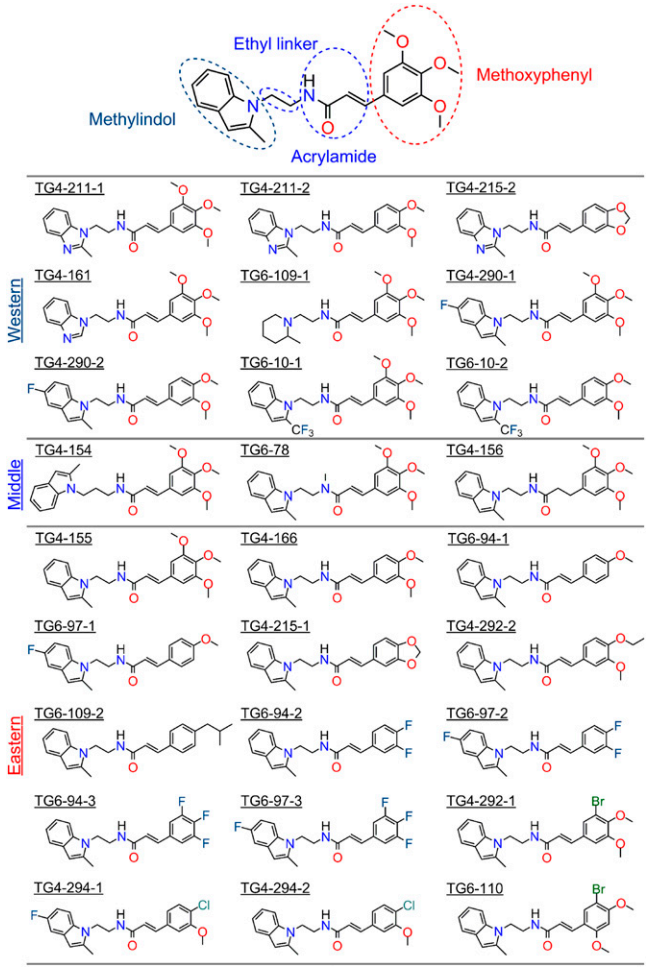

Fig. 3. Hit structure and analog design. Analogs were designed on the basis of the structure of hits TG4-155 and TG4-166.

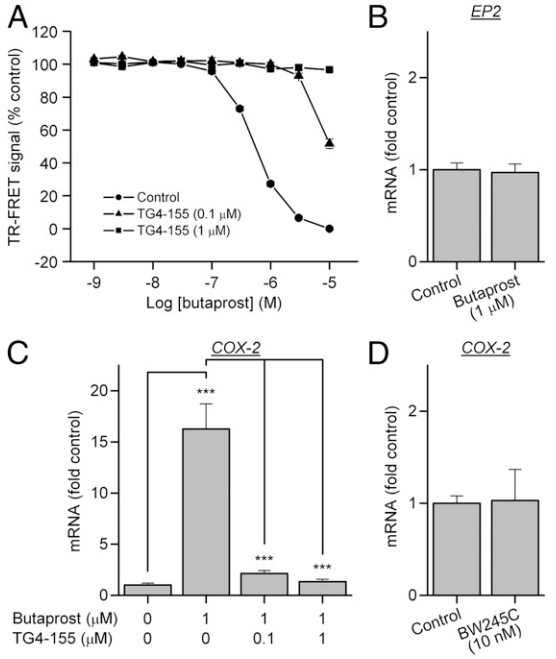

Fig. 4. EP2 activation induces microglial activation. (*A*) Butaprost increased cAMP levels in rat primary microglial cultures with EC_{50} = 0.5 μM. TG4-155 showed robust inhibition of butaprost-induced cAMP accumulation in rat microglia in a concentration-dependent manner, with potency equivalent to a Schild K_B = 5 nM. (*B*) EP2 activation in microglia by butaprost (1 μM) did not affect expression of the EP2 receptor itself in cultured microglia. (*C*) Butaprost (1 μM) induced COX-2 expression 16.3-fold above background in microglia, measured by quantitative real-time PCR (qRT-PCR). The COX-2 up-regulation was attenuated by TG4-155. (*D*) BW245C, a selective DP1 agonist, did not induce microglial COX-2 at 10 nM. Bars represent the mean ± SEM (n = 3–4). ***$P < 0.001$ by one-way ANOVA with posthoc Bonferroni.

DP1 agonist, PGD_2, from the induced mRNA. These considerations lead to the conclusion that TG4-155 blocks endogenous as well as recombinant EP2 and confirm a role for the EP2 signaling pathway in microglia.

Delayed Administration of EP2 Antagonist Reduces Neuronal Injury Induced by Status Epilepticus. Up-regulation of COX-2 in neuronal tissue after a seizure or cerebral ischemia usually contributes to neuronal injury. However, the downstream COX-2 signaling pathways involved in brain injury are not well known. Creation of potent antagonists of the human prostaglandin EP2 receptor provides a new opportunity to determine whether this key prostaglandin receptor plays a role in pathological conditions. Thus, we determined the effect of EP2 inhibition by these compounds after pilocarpine-induced SE in mice. First, we evaluated the potency of TG4-155 on mouse EP2 receptor because of sequence differences between human and mouse EP2. TG4-155 displayed robust inhibition of PGE_2-induced cAMP accumulation in C6G cells stably expressing mouse EP2 receptor (C6G-mEP2) in a dose-dependent manner with a K_B value of 4.7 nM, which is similar to that in human EP2 (Fig. S7). TG4-155 displayed a bioavailability of 61% (i.p. route compared with i.v.), a plasma half-life of 0.6 h, and a brain/plasma ratio of 0.3 in mice after i.p. administration (Fig. S8). Despite its short plasma half-life we felt it was worthwhile to test the effect of TG4-155 in an in vivo mouse model of epilepsy because COX-2 up-regulation after seizures is rapid.

Pilocarpine-induced SE was allowed to proceed for 1 h and then terminated by pentobarbital (*SI Materials and Methods*). The mice were then randomized and TG4-155 or vehicle was administered (5 mg/kg, i.p.) 1 h after termination of SE and then again 12 h later. The first injection was timed to overlap the early peak of neuronal COX-2 induction; given the brain half-life and the amount injected, the brain concentration of TG4-155 is predicted to be higher than the mouse K_B for >3 h (Fig. S8). Animals (10 in each group) were euthanized and the brains were collected 24 h after SE. To evaluate brain injury of mice, coronal brain sections (8 μm, three to nine sections per mouse throughout the hippocampus) were stained with Fluoro-Jade (0.001%, wt/vol) and scored for degenerating neurons in hippocampal subregions CA1, CA3, and dentate hilus (Fig. S9). Pilocarpine-induced SE caused substantial neurodegeneration in hippocampus 24 h after SE (Fig. 5*A*), whereas no positive staining was detected in animals from the control groups. Administration of TG4-155 significantly reduced SE-induced neurodegeneration scores by 91% ($P < 0.001$) in CA1, by 80% ($P < 0.01$) in CA3, and by 63% ($P < 0.001$) in hilus (Fig. 5*B*). The involvement of DP1 in the effect of TG4-155 should be very limited because TG4-155 had a concentration of ~69 nM in the mouse brain at 1 h after administration (Fig. S8) and thus would have had at most a very brief effect on DP1 (Fig. S3). Moreover, DP1 inhibition is proconvulsive in the pentylenetetrazol model (27), arguing against a prominent role for DP1 inhibition in the neuroprotection produced by TG4-155. However, DP1 activation can be neuroprotective in models of excitotoxicity and ischemia (28, 29), so whether DP1 activation by PGD_2 contributes to seizure-induced neuronal injury requires additional study. Further studies are also needed to optimize the TG4-155 treatment

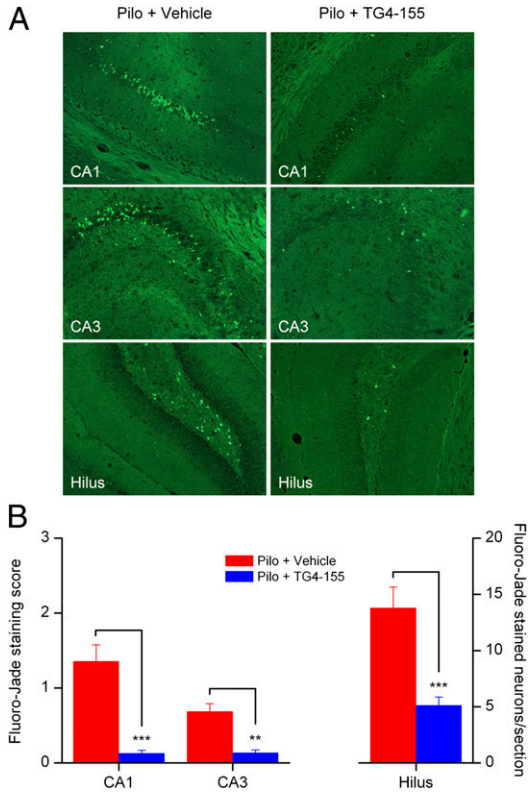

Fig. 5. EP2 inhibition reduced neuronal injury after SE. (*A*) Neurodegeneration in hippocampi from animals treated with vehicle or TG4-155 was assessed by Fluoro-Jade staining 24 h after SE. No positive staining was detected in control mice treated with vehicle or TG4-155. (*B*) Quantification of neurodegenerating neurons in hippocampal subregions CA1, CA3, and dentate hilus. Coronal brain sections from 10 animals in each group were examined with a fluorescence microscope. Neuron injury in CA1 and CA3 was quantified by averaging the injury scores from three to nine sections per mouse (in each section: 0, <3 Fluoro-Jade–positive cells; 1, 3–30 cells; 2, 31–100 cells; 3, extensive Fluoro-Jade staining), exemplified in Fig. S9. Neuron injury in the hilus was evaluated by counts of Fluoro-Jade–positive cells per section (n = 10 mice per group, $^{**}P < 0.01$, $^{***}P < 0.001$; one-way ANOVA and posthoc Bonferroni with selected pairs for CA1 and CA3, t test for hilus). Data are shown as mean ± SEM.

protocol (dose and dose intervals) to determine whether neuroprotection is sustained at longer time points (e.g., several weeks after SE) and to determine whether TG4-155 displays a direct anticonvulsant effect. However, these results provide strong support for involvement of the EP2 receptor in neuronal injury following a prolonged seizure.

Discussion

Sustained COX-2 activation in CNS can result in PGE_2-mediated brain inflammation and injury (2, 4, 5, 7, 20). For example, the EP1 prostaglandin receptor was reported to mediate COX-2–directed neurotoxicity in ischemic stroke (6), and EP2 accelerates the progression of experimental amyotrophic lateral sclerosis (10). EP2 is emerging as a principal mediator of brain inflammation after injury. Genetic ablation of prostanoid receptors has been useful but is complicated by the possibility of developmental and other homeostatic adjustments (9). Small molecules as selective modulators for prostaglandin receptors would be a valuable complement to genetic strategies. We now report discovery of a group of compounds that act as potent competitive antagonists of the human, mouse, and rat prostaglandin EP2 receptors. These compounds contain a 3-aryl-acrylamide scaffold and are structurally distinct from PF-04418948, a highly selective EP2 antagonist recently reported by Pfizer (21). The selectivity of PF-04418948 for EP2 over DP1 is higher than that of TG4-155; however, PF-04418948 was not tested as an inhibitor of COX-1 or COX-2, and its brain penetration was not reported. Identification of selective and potent antagonists of the EP2 receptor provides an opportunity to address the pathological functions of this key prostaglandin receptor to reach a more detailed understanding of the COX-2 cascade in disease.

The EP2 antagonists we report here have robust potency, good selectivity, and brain penetration. The most potent compounds showed competitive antagonism with K_B values of 2 nM against human EP2 in Schild regression analyses (Fig. 2 and Table 1). These EP2 inhibitors produced a similar effect on the butaprost and PGE_2 dose–response curves, indicating that their inhibition is not agonist specific (Fig. 1*C*), and they were effective on native EP2 receptors expressed by microglia (Fig. 4*A*). The results from secondary assays exclude possible effects of these compounds up- or downstream of the EP2 receptor. Their lack of effect on EP4 and β2-adrenergic receptors rules out a direct action on the Gαs protein, adenylate cyclase, phosphodiesterase, and the TR-FRET assay itself (Fig. S1 and Fig. 1 *D* and *E*). Both EP2 and EP4 receptors are Gαs coupled and elevate the cytoplasmic cAMP level in response to PGE_2 binding, which has made it difficult to distinguish EP2 from EP4 functions in conditions involving induced PGE_2 formation. The high selectivity (up to 4,730-fold) of these antagonists for EP2 over EP4 (Fig. 1*D* and Table 1) will make it feasible to address which PGE_2 receptor subtype is involved in Gαs-mediated inflammatory conditions. Furthermore, these compounds displayed very little or no detectable activity at other tested prostanoid receptors except the DP1 receptor, against which TG4-155 was 7-fold less potent than at EP2 (Fig. S3).

The mechanisms of COX induction and the roles of EP2 receptor activation in seizure-induced neuroinflammation and neurodegeneration are clearly multifactorial and likely cell specific. Studies of neuron-specific conditional knockouts of COX-2 demonstrate that neuronal induction of COX-2 triggers or exacerbates brain inflammation and neurodegeneration after pilocarpine (13). Microglial COX-1 is an alternative source of PGE_2 that might also play a role in brain inflammation (30, 31). As brain macrophages, microglia are a major mediator of immune responses in CNS and are effectors of brain inflammation and neurodegeneration in various models of neurological disorders (24). We hypothesize that after seizures neuronal COX-2 produces PGE_2, which activates EP2 receptors on microglia, accelerating the innate immune response after SE and triggering secondary neurodegeneration. At the same time, activation of EP2 receptors on neurons, via a PKA-dependent pathway, appears to be neuroprotective in acute models of NMDA-induced excitotoxicity and ischemia (3, 11, 12). The dual role of EP2 receptors, mediating both neuroprotection and neurodegeneration perhaps by different cell types and different pathways (32), complicates exploitation of EP2 as a therapeutic target. The balance between opposing NMDA-mediated cell injury and promoting injurious inflammation will likely be different for different neurologic disorders.

SE in man is associated with substantial mortality and morbidity that involve brain injury and inflammation. We demonstrate that inhibition of the EP2 receptor after SE was terminated significantly reduces neurodegeneration in mice assessed 24 h later (Fig. 5). This beneficial effect was not derived from conventional COX blockade because TG4-155 does not target COX-1 or COX-2 (Fig. S3) and was unlikely to involve the weaker inhibition of DP1 because the TG4-155 brain levels reached were too low. Neuroprotection by EP2 inhibition reveals a role for this key prostaglandin receptor in progression of seizure-induced neurodegeneration, possibly via induction of inflammatory mediators in microglia. The effect of EP2 antagonists on brain inflammation in other chronic neurologic disorders such as Alzheimer's and Parkinson's diseases awaits study.

Materials and Methods

Time-Resolved Fluorescence Resonance Energy Transfer (TR-FRET) cAMP Assay. cAMP was measured with a cell-based homogeneous TR-FRET method (Cisbio Bioassays). The assay is based on generation of a strong FRET signal upon the interaction of two molecules: an anti-cAMP antibody coupled to a FRET donor (Cryptate) and cAMP coupled to a FRET acceptor (d2). Endogenous cAMP produced by cells competes with labeled cAMP for binding to the cAMP antibody and thus reduces the FRET signal. Please see *SI Materials and Methods* for details.

Rat Primary Microglial Culture. Cortices from newborn Sprague–Dawley rats were carefully dissected, triturated, and washed. Cortical cells were cultured for 14 d with medium changed every 2–3 days. The loosely attached microglia were dislodged from the underlying astrocyte monolayer and collected. The cells were resuspended and plated on BD Primaria culture dishes or plates (BD Biosciences). Nonadherent cells were removed by changing the medium after 30–60 min. The adherent microglia were incubated for 24 h, underwent serum starvation for 24 h, and were then ready for use. Please see *SI Materials and Methods* for details.

Quantitative Real-Time Polymerase Chain Reaction (qRT-PCR). Rat primary microglial cultures were preincubated for 30 min with vehicle or test compound, followed by treatment with 1 μM butaprost or 10 nM BW245C for 2 h. Total RNA was isolated using TRIzol (Invitrogen) with the PureLink RNA Mini Kit (Invitrogen) from cultured cells. First-strand complementary DNA (cDNA) synthesis was performed with SuperScript II Reverse Transcriptase (Invitrogen). qRT-PCR was performed by using iQ SYBR Green Supermix (Bio-Rad Laboratories) in the iQ5 Multicolor Real-Time PCR Detection System (Bio-Rad Laboratories). Please see *SI Materials and Methods* for details.

Animals and Treatment. C57BL/6 mice (8–12 wk old) were injected with pilocarpine (280 mg/kg, i.p.) to induce status epilepticus (SE). SE was allowed for 1 h and terminated by pentobarbital (30 mg/kg, i.p.). Mice were then randomized by assignment to a random number stream and received two doses of vehicle or TG4-155 (5 mg/kg, i.p.) at 1 and 12 h after SE termination. Mice were euthanized under deep isoflurane anesthesia 24 h after SE and brains were collected for histology. Please see *SI Materials and Methods* for details.

Neuropathology. Fixed mouse brains (n = 10 per group) were sectioned (8 μm) coronally. Neurodegeneration in the hippocampus was assessed by Fluoro-Jade staining as previously described (13). Fluoro-Jade staining in each of three to nine sections (median: six sections) per mouse between bregma −1.22 and −3.52 was quantified in CA1 and CA3 by scoring criteria (0, <3 Fluoro-Jade–positive cells per section; 1, 3–30 cells; 2, 31–100 cells; 3, extensive Fluoro-Jade staining), exemplified in Fig. S9. The average injury score for each mouse was a continuous variable that ranged from 0.11 to 2.60 and was used to compare the degree of injury in mice treated with vehicle or TG4-155. The injury scores passed the Kolmogorov–Smirnov test for normality. Neuronal injury in the dentate hilus was measured by counts of Fluoro-Jade–positive cells in each section. Please see *SI Materials and Methods* for details.

Statistical Analysis. Data were plotted with Origin (OriginLab). Statistical analyses were performed using Prism (GraphPad Software) with one-way ANOVA and posthoc Bonferroni or t test as appropriate. $P < 0.05$ was considered to be statistically significant. Data were normalized to control (vehicle) values and presented as mean ± SEM.

ACKNOWLEDGMENTS. We appreciate the excellent technical assistance of Renee Shaw, Clinton Maddox, Iestyn Lewis, and Brian Revennaugh. This work was supported by Epilepsy Foundation Postdoctoral Research Fellowship 219142 (to J.J.); National Institutes of Health Grant R21NS074169 (to R.D.); and the CounterACT Program, Office of the Director, National Institutes of Health (OD) and the National Institute of Neurological Disorders and Stroke (NINDS), Grant U01NS058158 (to R.D.).

1. Kaufmann WE, Worley PF, Pegg J, Bremer M, Isakson P (1996) COX-2, a synaptically induced enzyme, is expressed by excitatory neurons at postsynaptic sites in rat cerebral cortex. *Proc Natl Acad Sci USA* 93:2317–2321.
2. Marcheselli VL, Bazan NG (1996) Sustained induction of prostaglandin endoperoxide synthase-2 by seizures in hippocampus. Inhibition by a platelet-activating factor antagonist. *J Biol Chem* 271:24794–24799.
3. McCullough L, et al. (2004) Neuroprotective function of the PGE2 EP2 receptor in cerebral ischemia. *J Neurosci* 24:257–268.
4. Nakayama M, et al. (1998) Cyclooxygenase-2 inhibition prevents delayed death of CA1 hippocampal neurons following global ischemia. *Proc Natl Acad Sci USA* 95: 10954–10959.
5. Iadecola C, et al. (2001) Reduced susceptibility to ischemic brain injury and N-methyl-D-aspartate-mediated neurotoxicity in cyclooxygenase-2-deficient mice. *Proc Natl Acad Sci USA* 98:1294–1299.
6. Kawano T, et al. (2006) Prostaglandin E2 EP1 receptors: Downstream effectors of COX-2 neurotoxicity. *Nat Med* 12:225–229.
7. Minghetti L (2004) Cyclooxygenase-2 (COX-2) in inflammatory and degenerative brain diseases. *J Neuropathol Exp Neurol* 63:901–910.
8. Abraham NS, El-Serag HB, Hartman C, Richardson P, Deswal A (2007) Cyclooxygenase-2 selectivity of non-steroidal anti-inflammatory drugs and the risk of myocardial infarction and cerebrovascular accident. *Aliment Pharmacol Ther* 25:913–924.
9. Hirata T, Narumiya S (2011) Prostanoid receptors. *Chem Rev* 111:6209–6230.
10. Liang X, et al. (2008) The prostaglandin E2 EP2 receptor accelerates disease progression and inflammation in a model of amyotrophic lateral sclerosis. *Ann Neurol* 64: 304–314.
11. Jiang J, et al. (2010) Neuroprotection by selective allosteric potentiators of the EP2 prostaglandin receptor. *Proc Natl Acad Sci USA* 107:2307–2312.
12. Liu D, Wu L, Breyer R, Mattson MP, Andreasson K (2005) Neuroprotection by the PGE2 EP2 receptor in permanent focal cerebral ischemia. *Ann Neurol* 57:758–761.
13. Serrano GE, et al. (2011) Ablation of cyclooxygenase-2 in forebrain neurons is neuroprotective and dampens brain inflammation after status epilepticus. *J Neurosci* 31: 14850–14860.
14. Yang H, Zhang J, Breyer RM, Chen C (2009) Altered hippocampal long-term synaptic plasticity in mice deficient in the PGE2 EP2 receptor. *J Neurochem* 108:295–304.
15. Liang X, et al. (2005) Deletion of the prostaglandin E2 EP2 receptor reduces oxidative damage and amyloid burden in a model of Alzheimer's disease. *J Neurosci* 25: 10180–10187.
16. Jin J, et al. (2007) Prostaglandin E2 receptor subtype 2 (EP2) regulates microglial activation and associated neurotoxicity induced by aggregated alpha-synuclein. *J Neuroinflammation*, 10.1186/1742-2094-4-2.
17. Hsiao HY, et al. (2007) TNF-alpha/IFN-gamma-induced iNOS expression increased by prostaglandin E2 in rat primary astrocytes via EP2-evoked cAMP/PKA and intracellular calcium signaling. *Glia* 55:214–223.
18. Hösl K, et al. (2006) Spinal prostaglandin E receptors of the EP2 subtype and the glycine receptor alpha3 subunit, which mediate central inflammatory hyperalgesia, do not contribute to pain after peripheral nerve injury or formalin injection. *Pain* 126: 46–53.
19. Reinold H, et al. (2005) Spinal inflammatory hyperalgesia is mediated by prostaglandin E receptors of the EP2 subtype. *J Clin Invest* 115:673–679.
20. Farooqui AA, Horrocks LA, Farooqui T (2007) Modulation of inflammation in brain: A matter of fat. *J Neurochem* 101:577–599.
21. af Forselles KJ, et al. (2011) In vitro and in vivo characterization of PF-04418948, a novel, potent and selective prostaglandin EP_2 receptor antagonist. *Br J Pharmacol* 164:1847–1856.
22. Jiang J, Ganesh T, Du Y, Quan Y, Dingledine R (2010) Novel selective antagonists reveal yin-yang nature of the prostaglandin EP2 receptor in brain injury. *Soc Neurosci Abstract Viewer and Itinerary Planner.* Available at http://www.abstractsonline.com/Plan/ViewAbstract.aspx?sKey=855950d5-ec4f-4899-819b-b706b8881f31&cKey=6c4117d5-9e19-485e-b5bd-03b3f3abb107&mKey=%7bE5D5C83F-CE2D-4D71-9DD6-FC7231E090FB%7d.
23. Jiang J, et al. (2011) Novel small molecule antagonists reveal a role of prostaglandin EP2 receptor in seizure-related neuronal injury and inflammation. *Soc Neurosci Abstract Viewer and Itinerary Planner.* Available at http://www.abstractsonline.com/Plan/ViewAbstract.aspx?sKey=aceb149d-00af-4c74-9a09-69314e726c7d&cKey=eefb3ecf-dbb0-476f-bc8e-3441a37bf194&mKey={8334BE29-8911-4991-8C31-32B32DD5E6C8}.
24. Perry VH, Nicoll JA, Holmes C (2010) Microglia in neurodegenerative disease. *Nat Rev Neurol* 6:193–201.
25. Li P, et al. (2009) Expression of cyclooxygenase-1/-2, microsomal prostaglandin-E synthase-1 and E-prostanoid receptor 2 and regulation of inflammatory mediators by PGE(2) in the amoeboid microglia in hypoxic postnatal rats and murine BV-2 cells. *Neuroscience* 164:948–962.
26. Abramovitz M, et al. (2000) The utilization of recombinant prostanoid receptors to determine the affinities and selectivities of prostaglandins and related analogs. *Biochim Biophys Acta* 1483:285–293.
27. Akarsu ES, Mamuk S, Comert A (1998) Inhibition of pentylenetetrazol-induced seizures in rats by prostaglandin D2. *Epilepsy Res* 30:63–68.
28. Liang X, Wu L, Hand T, Andreasson K (2005) Prostaglandin D2 mediates neuronal protection via the DP1 receptor. *J Neurochem* 92:477–486.
29. Taniguchi H, et al. (2007) Prostaglandin D2 protects neonatal mouse brain from hypoxic ischemic injury. *J Neurosci* 27:4303–4312.
30. Deininger MH, Schluesener HJ (1999) Cyclooxygenases-1 and -2 are differentially localized to microglia and endothelium in rat EAE and glioma. *J Neuroimmunol* 95: 202–208.
31. Yermakova AV, Rollins J, Callahan LM, Rogers J, O'Banion MK (1999) Cyclooxygenase-1 in human Alzheimer and control brain: Quantitative analysis of expression by microglia and CA3 hippocampal neurons. *J Neuropathol Exp Neurol* 58:1135–1146.
32. Quan Y, Jiang J, Dingledine R (2011) Signaling pathways for EP2 receptors regulate microglial activation. *Society Neurosci Abstract Viewer and Itinerary Planner.* Available at http://www.abstractsonline.com/Plan/ViewAbstract.aspx?sKey=3b5856f9-dbbd-4ef6-9834-e8a538e84bf5&cKey=aed366a6-adeb-4d0d-ad4d-106fb01ca5eb&mKey=%7b8334BE29-8911-4991-8C31-32B32DD5E6C8%7d.

Supporting Information

Jiang et al. 10.1073/pnas.1120195109

SI Results

High-Throughput Screening for EP2 Antagonists. Using a cell-based time-resolved fluorescence resonance energy transfer (TR-FRET) assay to monitor prostaglandin E2 receptor (PGE_2)-induced cAMP accumulation in human EP2-overexpressing C6 glioma (C6G-EP2) cells (1), we screened a library of 262,371 small molecules (each at 20 μM in singlicate) for compounds that increase the TR-FRET signal (i.e., decrease the cytoplasmic cAMP level) in the presence of 1 μM PGE_2 in C6G-EP2 cells (Fig. S1*A*). The concentration of 1 μM PGE_2 is 500- to 1,000-fold higher than its EC_{50} in this assay (typically 1–2 nM) and therefore saturates the EP2 receptor response to the agonist. Two measures of assay robustness, the signal-to-noise ratio (*S*/*N*) and the *Z*-factor, were used to ensure quality of the assay for screening. Both assay parameters were adequate for high-throughput screening (HTS) ($S/N > 4.5$, Z-factor > 0.5) over the primary screening (Fig. S2). A total of 656 compounds inhibited the response of C6G-EP2 cells to PGE_2 by at least 55% at 20 μM and were further tested in dose–response in triplicate in a suite of four secondary assays designed to eliminate false positives and evaluate selectivity: (*i*) inhibition of PGE_2 (1 μM)-induced cAMP accumulation in C6G-EP2 cells, (*ii*) inhibition of PGE_2 (1 μM)-induced cAMP accumulation in HEK-EP4 cells, (*iii*) inhibition of isoproterenol (1 μM)-induced cAMP accumulation in C6G-β2-adrenergic receptor cells, and (*iv*) increasing the TR-FRET signal in a cell-free system in the presence of 1 μM cAMP (Fig. S1*A*). Compounds had to be positive in the first assay (IC_{50} < 10 μM) and negative in assays *ii* and *iii* (<40% maximum inhibition) without affecting the assay itself (*iv*) to proceed. Assays *ii* and *iii* are designed to examine selectivity because, like EP2, both EP4 and β2-adrenergic receptors couple through Gαs to stimulate adenylate cyclase; a negative response in these assays also minimizes the possibility that a compound reduces cAMP by directly activating phosphodiesterase. Inactivity in assay *iv* demonstrates that the compound does not interfere with the assay itself, for example by directly elevating the TR-FRET signal. A total of 13 compounds passed the secondary assays and an extra confirmatory test (*i*) (Fig. S1*A*). Among those, hits PubChem substance identification number (SID) 17,515,129 (resynthesized as TG4-155) and SID 17,515,102 (TG4-166) are the most potent compounds and showed robust inhibition of PGE_2 (1 μM)-induced cAMP accumulation in C6G-EP2 cells without affecting EP4 or β2-adrenergic receptors under agonist-saturated conditions (Fig. S1*B*).

Structure–Activity Relationships. In the western side of the molecule, addition of an extra nitrogen in the indol ring to improve solubility, as in TG4-211-1, TG4-211-2, TG4-215-2, and TG4-161, significantly reduced the potency of the compound (Table 1). Substitution of the indol ring by a methylpiperidine ring (TG6-109-1) eliminated activity. A fluorine attached to the methylindol ring (TG4-290-1 and TG4-290-2) did not significantly affect the compound potency. If the methylindol ring was replaced by trifluoromethylindol, as in TG6-10-1 and TG6-10-2, compound potency was reduced only ~10-fold. Thus, incorporation of a fluorine or trifluoromethyl group is well tolerated, which is potentially useful to improve compound pharmacokinetic properties (2). In the central portion of the molecule, replacement of the ethyl with propyl (TG4-154) to lengthen the linker between acrylamide and methylindol, or addition of *N*-methyl to the acrylamide (TG6-78), or replacement of acrylamide by propionamide (TG4-156) to remove the double bond greatly diminished potency. In the eastern side of the molecule, potency followed the pattern trimethoxyphenyl (TG4-155) > dimethoxyphenyl (TG4-166) > monomethoxyphenyl (TG6-94-1 and TG6-97-1) > benzodioxole (TG4-215-1). If a methoxy was replaced by ethoxy (TG4-292-2), potency was not much affected. However, if the methoxy was replaced by an isobutyl (TG6-109-2), potency was reduced about fivefold compared with TG6-94-1. Interestingly, if the methoxy was replaced by fluorine, the potency from difluorophenyl (TG6-94-2 and TG6-97-2) is higher than that from trifluorophenyl (TG6-94-3 and TG6-97-3). Replacement of methoxy by other halogens such as bromine in TG4-292-1, or chlorine in TG4-294-1 and TG4-294-2, also increased potency compared with TG4-155, TG4-166, and TG4-290-2. The methoxy position in the phenyl ring is also critical for the compound activity; for example, if methoxy was rotated from the 3 to the 2 position, inhibition was significantly reduced, comparing TG4-292-1 to TG6-110.

SI Materials and Methods

Cell Culture. The rat C6 glioma (C6G) cells stably expressing human EP2 (C6G-EP2) or mouse EP2 (C6G-mEP2) receptors were created in the laboratory (1) and grown in Dulbecco's modified Eagle medium (DMEM) (Invitrogen), supplemented with 10% (vol/vol) FBS (Invitrogen), 100 units/mL penicillin, 100 μg/mL streptomycin (Invitrogen), and 0.5 mg/mL G418 (Invitrogen). The human embryonic kidney (HEK) cell line stably expressing the human EP4 receptors (HEK-EP4) was a kind gift from Merck. The C6G cell line stably expressing β2-adrenergic receptors (C6G-β2-AR) was a kind gift from Kenneth Minneman from Emory University (Atlanta, GA). HEK-EP4 cells and C6G-β2-AR cells were maintained in complete DMEM containing 250 μg/mL G418 and 200 μg/mL hygromycin B (Invitrogen).

Chemicals and Drugs. PGE_2, butaprost, BW245C, rolipram, and doxorubicin were purchased from Cayman Chemical. Isoproterenol, methylscopolamine, terbutaline, pilocarpine, and pentobarbital were purchased from Sigma-Aldrich.

HTS in 1,536-Well Format. C6G-EP2 cells were dissociated and suspended in Hanks' buffered salt solution (HBSS). To optimize cell density for HTS and minimize day-to-day variation, a dose–response curve for PGE_2 was obtained at several cell densities every day before screening. The cell density (generally 2,000–3,000 cells per well) yielding an EC_{50} for PGE_2 of 2–3 nM was selected for HTS. Assay plates were prepared by dispensing 4 μL per well of the cells suspended in HBSS containing 20 μM rolipram into 1,536-well black plates (Corning), using a Multidrop Combi dispenser (Thermo-Fisher Scientific). One-tenth microliter of 1 mM library compounds diluted in DMSO or vehicle was transferred to the cell assay plate, using a Pintool (V&P Scientific) integrated with Beckman NX liquid handler (Beckman Coulter), and incubated for 5–30 min. Then, 1 μL of 5 μM PGE_2 was dispensed to the wells with library compounds or vehicle as a control. The final concentration of the library compound was 20 μM and the PGE_2 concentration was 1 μM. Each plate had a set of positive and negative controls in one 32-well column. After incubating with PGE_2 for 30 min, the cAMP-d2 (1 μL) and anti–cAMP-Cryptate (2 μL) in lysis buffer were dispensed sequentially to the assay plates and incubation continued at room temperature for 0.5–2 h. The TR-FRET signal was measured by an Envision 2103 Multilabel Plate Reader (PerkinElmer Life Sciences) with a laser excitation at 337 nm and dual emissions at 665 nm and 590 nm for d2 and Cryptate, respectively. The FRET signal is expressed as $F665/F590 \times 10^4$. The effect of

each compound on 1 μM PGE_2-induced cAMP production was expressed by the following equation:

$$\%\ \text{inhibition of } PGE_2\text{-induced cAMP} = 100 - 100 \times (\text{FRET signal from vehicle} - \text{FRET signal from test compound with } PGE_2)/(\text{FRET signal from vehicle} - \text{FRET signal from } PGE_2 \text{ only}).$$

All screening data were deposited into PubChem (http://pubchem.ncbi.nlm.nih.gov/, assay ID 1422).

cAMP Assay in 384-Well Format. Cells were seeded into 384-well plates in 30 μL complete medium (4,000 cells per well) and grown overnight. The medium was thoroughly withdrawn and 10 μL HBSS (HyClone) plus 20 μM rolipram were added into the wells to block phosphodiesterase. The cells were incubated at room temperature for 30 min and then treated with vehicle or test compound for 5 min before addition of increasing concentrations of appropriate agonist-PGE_2, butaprost, or isoproterenol for 40 min. The cells were lysed in 10 μL lysis buffer containing the FRET acceptor cAMP-d2 and 1 min later another 10 μL lysis buffer with anti–cAMP-Cryptate was added. After 60–90 min incubation at room temperature, the TR-FRET signal was detected by an Envision 2103 Multilabel Plate Reader (PerkinElmer) with a laser excitation at 337 nm and dual emissions at 665 nm and 590 nm for d2 and Cryptate, respectively. The FRET signal is expressed as $F665/F590 \times 10^4$.

Radioligand Binding Assay. Binding selectivity assays for EP2 receptor were performed at Cerep. Cell membrane homogenates (20 μg protein) from HEK cells stably expressing human EP2 receptor were incubated with 3 nM [^{3}H]PGE_2 in the absence or presence of the test compound in a buffer containing 10 mM Mes/KOH (pH 6.0), 10 mM $MgCl_2$, and 1 mM EDTA, at room temperature for 120 min. Nonspecific binding was determined in the presence of 10 μM PGE_2. Following incubation, the samples were filtered rapidly under vacuum through glass fiber filters (GF/B; Packard) presoaked with 0.3% polyethyleneimine (PEI) and rinsed several times with ice-cold 50 mM Tris·HCl, using a 96-sample cell harvester (UniFilter; Packard). The filters were dried and then counted for radioactivity in a scintillation counter (TopCount; Packard), using a scintillation mixture (MicroScint 0; Packard). The results were expressed as a percentage of inhibition of the control radioligand-specific binding. The dose–response curves were generated, and IC_{50} and K_i values were calculated with Origin (OriginLab).

Cellular Functional Assays in Recombinant Cells. Broad spectrum selectivity assays of TG4-155 were carried out by Cerep. In brief, Chinese hamster ovary (CHO) cells or HEK cells stably expressing human BLT1, DP1, EP1, EP2, EP3, EP4, FP, IP or TP were preincubated with or without test compound at room temperature for 5 min, and then an EC_{80} of specific reference agonist, i.e., 10 nM LTB_4 for BLT1, 10 nM BW245C for DP1, 3 nM PGE_2 for EP1, 300 nM PGE_2 for EP2, 0.1 nM sulprostone for EP3, 30 nM PGE_2 for EP4, 5 nM $PGF_{2\alpha}$ for FP, 0.3 nM iloprost for IP, and 30 nM U-44069 for TP, was added to induce receptor response. Results were expressed as a percentage of inhibition of the control response to reference agonist. The dose–response curves were generated and IC_{50} values were calculated with Origin.

Enzyme Assay. Enzyme assays for COX-1 and COX-2 were performed by measuring the formation of PGE_2 from arachidonic acid at Cerep. COX-1 or COX-2 enzyme (0.2 μg) extracted from transfected Sf9 cells was preincubated with or without test compound in a buffer containing 90 mM Tris·HCl (pH 8.0), 1.98 mM phenol, and 1.02 μM hematine, at room temperature for 20 min. The reaction was initiated by adding 2 μM arachidonic acid, and the mixture was incubated at room temperature for 5 min. The reaction was stopped by adding 1 M HCl and then 1 M Tris·HCl (pH 8.0) followed by cooling to 4 °C. Production of PGE_2 was measured and the results were expressed as a percentage of inhibition of the control enzyme activity.

Metabolic Stability. In vitro metabolic stability assays were performed at SRI International. Test compounds (1 or 10 μM) were incubated with pooled human or mouse liver microsomes. Samples were collected at 0, 15, 30, and 60 min. The remaining parent compound in the solution was measured by liquid chromatography–mass spectrometry (LC-MS/MS). Heat-inactivated microsomes were used as negative controls in which no degradation of test compounds was detected.

Cytotoxicity Assay. Cytotoxicity of test compounds was examined with the CellTiter-Glo Luminescent Cell Viability Assay (Promega) by measuring cellular ATP level, which correlates with cell viability. Briefly, C6G cells were plated in 384-well plates at 2,000 cells per well in 25 μL DMEM plus test compound at increasing concentrations and incubated for 48 h. CellTiter-Glo reagent (25 μL) was then added to each well. The contents were mixed for 2 min on an orbital shaker to induce cell lysis and incubated at room temperature for 10 min. Relative viability is proportional to luminescence intensity as measured by a microplate reader (Molecular Devices) with an integration time of 1 s.

Rat Primary Microglial Culture. Cortices from newborn Sprague–Dawley rats were carefully dissected, triturated, and washed. Cortical cells were cultured in DMEM plus 10% FBS, 100 units/mL penicillin, 100 μg/mL streptomycin, and 2 ng/mL granulocyte–macrophage colony-stimulating factor (GM-CSF) for 14 d with medium changed every 2–3 d. The loosely attached microglia were dislodged from the underlying astrocyte monolayer by gentle agitation and then collected by centrifuge (300 × *g*, 10 min). The cells were resuspended in DMEM plus 10% FBS with penicillin/streptomycin and 0.2 ng/mL GM-CSF and plated on BD Primaria culture dishes or plates (BD Biosciences). Nonadherent cells were removed by changing the medium after 30–60 min. The adherent microglia were incubated for 24 h and underwent serum starvation in macrophage serum-free medium (MSFM) plus 0.2 ng/mL GM-CSF for 24 h. The purified microglia were then ready for use.

Quantitative Real-Time PCR (qRT-PCR). Primary microglial cultures were preincubated for 30 min with vehicle or test compound, followed by treatment with 1 μM butaprost or 10 nM BW245C for 2 h. Total RNA was isolated using TRIzol (Invitrogen) with the PureLink RNA Mini Kit (Invitrogen) from cultured cells. RNA concentration and purity were measured by A_{260} value and A_{260}/A_{280} ratio, respectively. First-strand cDNA synthesis was performed with 0.2 μg of total RNA, 200 units of SuperScript II Reverse Transcriptase (Invitrogen), and 0.5 μg random primer in a reaction volume of 30 μL at 42 °C for 50 min. The reaction was terminated by heating at 70 °C for 15 min. qRT-PCR was performed by using 8 μL of 10× diluted cDNA, 0.1–0.5 μM of primers, and 2× iQ SYBR Green Supermix (Bio-Rad Laboratories) with a final volume of 20 μL in the iQ5 Multicolor Real-Time PCR Detection System (Bio-Rad Laboratories). Cycling conditions were as follows: 95 °C for 2 min followed by 40 cycles of 95 °C for 15 s and then 60 °C for 1 min. Melting curve analysis was used to verify single-species PCR product. Fluorescent data were acquired at the 60 °C step. The geometric mean of cycle thresholds for β-actin, GAPDH, and HPRT1 was used as an internal control for relative quantification. Samples without cDNA template served as the negative controls.

Pharmacokinetics. Pharmacokinetics study of compound TG4-155 was performed at Absorption Systems. C57BL/6 mice (Charles River) were administered test compounds (3 mg/kg, i.p.) in formulation [5% dimethylacetamide (DMA), 50% PEG 400, 40% saline]. Blood samples were collected at 0.25, 0.5, 1, 2, 4, and 8 h, and the brain samples were collected at 0.5, 1, and 4 h. Three animals were used per time point and killed after a single blood collection. Plasma and brain homogenate samples were extracted and analyzed by LC-MS/MS.

Animals and Treatment. C57BL/6 mice (8–12 wk) from Charles River were housed under a 12-h light/dark cycle with food and water ad libitum. To minimize peripheral side effects of pilocarpine, mice were injected with methylscopolamine and terbutaline (2 mg/kg each in saline, i.p.). After 15–30 min, pilocarpine (280 mg/kg in saline, freshly prepared, i.p.) was injected to induce status epilepticus (SE). Control mice received methylscopolamine and terbutaline but no pilocarpine. Seizures were classified as follows (3–6):

Score	Motor behavior
0	Normal behavior: walking, exploring, sniffing, grooming
1	Immobile, staring, jumpy, curled-up posture
2	Automatisms: repetitive blinking, chewing, head bobbing, vibrissae twitching, scratching, face washing, "star gazing"
3	Partial body clonus or occasional myoclonic jerks, shivering
4	Whole body clonus, "corkscrew" turning and flipping; loss of posture, rearing, and falling
5	SE onset: nonintermittent seizure activity (usually stage 3 and/or 4 repeatedly)
6	Wild running and bouncing, tonic seizures
7	Death

Mice underwent SE for 1 h, and SE was then terminated by i.p. injection of 30 mg/kg pentobarbital in saline. Mice were then randomized by assignment to a random number stream and received two doses of vehicle (10% DMSO, 50% PEG 400, 40% ddH_2O) or TG4-155 (5 mg/kg, i.p.) at 1 and 12 h after SE termination. After mice became ambulatory, 0.5 mL 5% dextrose in lactated Ringer's solution (Baxter) was injected s.c. Mice were fed moistened high-fat rodent chow and injected s.c. with 0.5 mL 5% dextrose in lactate Ringer's solution when necessary. Mice were euthanized under deep isoflurane anesthesia 24 h after SE and brains were collected. The brains were immersed in 4% paraformaldehyde (PFA) fixative for at least 10 h for histology. All experiments were approved by the Institutional Animal Care and Use Committee of Emory University and conducted in accordance with its guidelines. Every effort was made to minimize animal suffering.

Neuropathology. Fixed mouse brains (n = 10 per group) were embedded in paraffin and sectioned (8 μm) coronally. Neurodegeneration in the hippocampus was assessed by Fluoro-Jade staining with a fluorescence microscope as described in ref. 6. Fluoro-Jade staining in each of three to nine sections (median: six sections) per mouse between bregma −1.22 and −3.52 was quantified in CA1 and CA3 by scoring criteria (0, <3 Fluoro-Jade–positive cells per section; 1, 3–30 cells; 2, 31–100 cells; 3, extensive Fluoro-Jade staining, often in patches), exemplified in Fig. S9. The average injury score for each mouse was a continuous variable that ranged from 0.11 to 2.60 and was used to compare the degree of injury in mice treated with vehicle or TG4-155. The injury scores passed the Kolmogorov–Smirnov test for normality. Neuronal injury in the dentate hilus was measured by counts of Fluoro-Jade–positive cells in each section. The evaluation of cell injury was done without knowledge of treatment.

Chemical Design and Synthesis. All compounds were either obtained through commercial sources or synthesized and analyzed by NMR, high-resolution mass spectrometry (HRMS), and elemental analysis. Agilent LC-MS was used to demonstrate that compounds did not degrade throughout the study. TG4-155 was synthesized as shown in Fig. S4. A solution of (E)-3-(3,4,5-trimethoxyphenyl) acrylic acid [220 mg, 0.92 mmol, 1.05 equivalent (eq.)] and dimethylaminopyridine (DMAP) (10 mg) in dichloromethane (6 mL) was added to a solution of 2-(2-methyl-1H-indol-1-yl)ethanamine (152 mg, 0.87 mmol, 1 eq.) in dichloromethane (2 mL), followed by 1-ethyl-3-(3-dimethylaminopropyl) carbodiimide hydrochloride (EDCI) (190 mg, 1 mmol, 1.13 eq.) at room temperature. The resulting solution was stirred for 3 h. At the conclusion of the reaction (monitored by TLC), water (25 mL) was added to quench the reaction. The organics were separated from aqueous phase by extraction with ethyl acetate (3×, 20 mL). Combined organics were washed with 1% HCl (10 mL), saturated $NaHCO_3$ solution (10 mL), water (10 mL), and brine solution (10 mL). Organics were dried and concentrated to dryness. The resulting crude product was recrystallized with hexane-ethyl acetate mixture to furnish pure compound product TG4-155 (300 mg, 85% yield). All other compounds were synthesized and characterized in a similar manner.

Mass spectrometric analysis was provided by the Emory University Mass Spectrometry Center. Proton NMR spectra were recorded in solvent deuteriochloroform ($CDCl_3$) on a Varian Inova-400 (400 MHz), unless otherwise mentioned. TLC was performed on precoated, aluminum-backed plates (silica gel 60 F_{254}, 0.25 mm thickness) from EM Science and was visualized by UV lamp. Column chromatography was performed with silica gel (230–400 mesh ASTM), using the "flash" method. Agilent LC-MS was used to measure purity of the products. Elemental analyses were performed by Atlantic Microlab.

TG4-155: ^{1}H NMR. δ 7.51 (d, J = 6.8 Hz, 1H), 7.48 (d, J = 15.6 Hz, 1H), 7.29 (d, J = 8 Hz, 1H), 7.10 (m, 2H), 6.66 (s, 2H), 6.24 (s, 1H), 6.14 (d, J = 15.6 Hz, 1H), 5.6 (t, J = 6 Hz, 2H), 4.3 (t, J = 6 Hz, 2H), 3.84 (s, 9H), 3.71 (q, J = 6 Hz, 2H), 2.39 (s, 3H). Anal. Calcd for $C_{23}H_{26}N_2O_4$: C, 70.03; H, 6.64; N, 7.10. Found: C, 69.61; H, 6.61; N, 7.04.

TG4-166: ^{1}H NMR. δ 7.52 (d, J = 15.6 Hz, 1H), 7.49 (d, J = 8 Hz, 1H), 7.26 (d, J = 8 Hz, 1H), 7.05 (m, 3H), 6.92 (d, J = 2 Hz, 1H), 6.77 (d, J = 8.4 Hz, 1H), 6.21 (s, 1H), 6.11 (d, J = 15.2 Hz, 1H), 5.89 (t. J = 6 Hz, 1H), 4.22 (t, J = 6 Hz, 2H), 3.84 (s, 3H), 3.81 (s, 3H), 3.58 (q, J = 6 Hz, 2H), 2.36 (s, 3H). Anal. Calcd for $C_{22}H_{24}N_2O_3$: C, 72.50; H, 6.64; N, 7.69. Found: C, 72.54; H, 6.70; N, 7.66.

TG4-211-1: ^{1}H NMR. δ 7.64 (m, 1H), 7.53 (d, J = 15.6 Hz, 1H), 7.3 (m, 1H), 7.20 (m, 2H), 6.6 (s, 2H), 6.20 (d, J = 15.6 Hz, 1H), 6.06 (m, 1H), 4.36 (t, J = 6 Hz, 2H), 3.84 (s, 9H), 3.75 (q, J = 5.6 Hz, 2H), 2.5 (s, 3H). HRMS Calcd for $C_{22}H_{26}N_3O_4$ (M+H): 396.19178. Found: 396. 19136.

TG4-211-2: ^{1}H NMR. δ 7.64 (m, 1H), 7.57 (d, J = 15.6 Hz, 1H), 7.31 (m, 1H), 7.19 (m, 2H), 7.04 (dd, J = 8.4, 2 Hz, 1H), 6.95 (d, J = 2Hz, 1H),6.82 (d, J = 8.4 Hz, 1H), 6.17 (d, J = 15.6 Hz, 1H), 6.08 (s, 1H), 4.35 (t, J = 6 Hz, 2H), 3.83 (s, 3H), 3.85 (s, 3H), 3.73 (q, J = 6 Hz, 2H), 2.49 (s, 3H). Anal. Calcd for $C_{21}H_{23}N_3O_4$: C, 69.02; H, 6.34; N, 11.50. Found: C, 68.77; H, 6.40; N, 11.32.

TG4-215-2: ^{1}H NMR. δ 7.56 (m, 1H), 7.45 (d, J = 15.6 Hz, 1H), 7.29 (m, 1H), 7.16 (m, 2H), 6.90 (s, 1H), 6.89 (s, 1H), 6.72 (dd, J = 8.4, 2 Hz, 1H), 6.1 (d, J = 15.6 Hz, 1H), 5.92 (s, 2H), 4.28 (t, J = 5. 6 Hz, 2H), 3.61 2.45 (s, 3H). HRMS Calcd for $C_{20}H_{20}N_3O_3$ (M+H): 350.14992. Found: 350.14960.

TG4-161: ^{1}H NMR. δ 7.57 (d, J = 7.2 Hz, 1H), 7.56 (s, 1H), 7.51 (d, J = 16 Hz, 1H), 7.37 (d, J = 8 Hz, 1H), 7.29 (t, J = 6 Hz, 1H), 7.20 (t, J = 7.6 Hz, 1H), 7.15 (t, J = 8 Hz, 1H), 6.59 (s, 2H), 6.33 (d, J = 15.6 Hz, 1H), 4.34 (t, J = 5.2 Hz, 2H), 3.80 (s, 3H), 3.72 (s. 6H). HRMS Calcd for $C_{21}H_{24}N_3O_4$ (M+H): 382.17613. Found: 382.17569.

TG6-109-1: ^{1}H NMR. δ 7.50 (d, J = 15.6 Hz, 1H), 6.89 (s, 1H), 6.70 (s, 2H), 6.34 (d, J = 15.6 Hz, 1H), 3.82 (s, 3H), 3.55 (m, 1H), 3.43 (m, 1H), 2.98 (m, 2H), 2.48 (m, 2H), 2.27 (m, 1H), 1.66 (m, 4H), 1.35 (m, 2H), 1.11 (d, J = 6.4 Hz, 3H). HRMS Calcd for $C_{20}H_{31}N_2O_4$ (M+H): 363.22783. Found: 363.22741.

TG4-290-1: ^{1}H NMR. δ 7.48 (d, J = 15.6 Hz, 1H), 7.18 (dd, J = 8.8, 4.4 Hz, 1H), 7.13 (dd, J = 9.6, 2.4 Hz, 1H), 6.84 (t x d, J = 8.8, 2.4 Hz, 1H), 7.63 (s, 2H), 6. 20 (s, 1H), 6.15 (d, J = 15.6 Hz, 1H), 5. 6 (t, J = 5.6 Hz, 1H), 4. 28 (t, J = 6.4 Hz, 1H), 3.84 (s, 9H), 3.67 (q, J = 6 Hz, 2H), 2.38 (s, 3H). Anal. Calcd for $C_{23}H_{25}FN_2O_4$: C, 66.98; H, 6.11; N, 6.79. Found: C, 66.93; H, 6.03; N, 6.69.

TG4-290-2: ^{1}H NMR. δ 7.52 (d, J = 15.6 Hz, 1H), 7.18 (dd, J = 8.8, 4.4 Hz, 1H), 7.13 (dd, J = 9.6, 2.4 Hz, 1H), 7.02 (dd, J = 8.2, 1.6 Hz, 1H), 6.94 (dd, J = 2 Hz, 1H),6.83 (m, 2H), 6. 17 (s, 1H), 6.12 (d, J = 15.6 Hz, 1H), 4. 2 (t, J = 6 Hz, 1H), 3.87 (s, 3H), 3.85 (s, 3H), 3.63 (q, J = 6 Hz, 2H), 2.37 (s, 3H). Anal. Calcd for $C_{22}H_{23}FN_2O_3$: C, 69.09; H, 6.06; N, 7.33. Found: C, 68.89; H, 6.01; N, 7.20.

TG6-10-1: ^{1}H NMR. δ 7.59 (d, J = 8 Hz, 1H), 7.54 (d, J = 8.4, Hz, 1H), 7.50 (d, J = 15.2 Hz, 1H), 7.27 (q, J = 7.2 Hz, 1H), 7.1 (t, J = 7. 2 Hz, 1H), 6.89 (s, 1H), 6. 63 (s, 2H), 6.4 (t, J = 6 Hz, 1H), 6. 25 (d, J = 15.2 Hz, 1H), 4.4 (t, J = 6.4 Hz, 1H), 3.8 (s, 3H), 3.76 (s, 6H), 3.69 (q, J = 6.4 Hz, 2H). Anal. Calcd for $C_{23}H_{23}F_3N_2O_4$: C, 61.60; H, 5.17; N, 6.25. Found: C, 61.34; H, 5.10; N, 6.16.

TG6-10-2: ^{1}H NMR. δ 7.62 (d, J = 8 Hz, 1H), 7.56 (d, J = 8.4, Hz, 1H), 7.55 (d, J = 15.6 Hz, 1H), 7.29 (t, J = 8 Hz, 1H), 7.13 (t, J = 7. 6 Hz, 1H), 7.0 (dd, J = 8.6, 2 Hz), 1H), 6. 93 (s, 2H), 6.79 (d, J = 8 Hz, 1H), 6. 17 (d, J = 15.6 Hz, 1H), 6.09 (t, J = 5.6 Hz, 1H), 4.4 (t, J = 6 Hz, 1H), 3.84 (s, 3H), 3.81 (s, 3H), 3.70 (q, J = 6 Hz, 2H). Anal. Calcd for $C_{22}H_{21}F_3N_2O_4$: C, 63.15; H, 5.06; N, 6.70. Found: C, 63.14; H, 5.94; N, 6.66.

TG4-154: ^{1}H NMR. δ 7.51 (d, J = 7.6 Hz, 1H), 7.34 (d, J = 15.6 Hz, 1H), 7.27 (d, J = 8 Hz, 1H), 7.13 (t, J = 7.6 Hz, 1H), 7.05 (t, J = 8 Hz, 1H), 6.65 (s, 2H), 6.24 (s, 1H), 6.0 (d, J = 15.6 Hz, 1H), 5.23 (s, 1H), 4.18 (t, J = 6.8 Hz, 2H), 3.87 (s, 6H), 3.85 (s, 3H), 3.04 (q, J = 6 Hz, 2H), 2.42 (s, 3H), 2.03 (q, J = 6.8 Hz, 2H). Anal. Calcd for $C_{24}H_{28}N_2O_4$: C, 70.57; H, 6.91; N, 6.86. Found: C, 70.37; H, 6.94; N, 6.80.

TG6-78: Proton signals were doubled, due to a quaternary nitrogen atom next to double bond, indicating a mixture of two stereoisomers. LCMS: *m/z*, 409 (M+H) (95% pure). HRMS Calcd for $C_{24}H_{28}N_2O_4$ (M+K): 447.16807; Found 447.16780.

TG4-156: ^{1}H NMR. δ 7.48 (d, J = 7.6 Hz, 1H), 7.20 (d, J = 8 Hz, 1H), 7.10 (t, J = 7.6 Hz, 1H), 7.04 (t, J = 8 Hz, 1H), 6.34 (s, 2H), 6.20 (s, 1H), 5.67 (t, J = 6 Hz, 1H), 4.13 (t. J = 6 Hz, 2H), 3.77 (s, 9H), 3.47 (q, J = 6 Hz, 2H), 2.80 (t, J = 7.6 Hz, 2H), 2.34 (s, 3H), 2.30 (t, J = 7.2 Hz, 2H). HRMS Calcd for $C_{23}H_{29}N_2O_4$ (M+H): 397.21218. Found: 397. 21177.

TG6-94-1: ^{1}H NMR ($CDCl_3$ + drops of MeOH-d_4) δ 7.46 (d, J = 15.6 Hz, 1H), 7.44 (d, J = 7.2 Hz, 1H), 7.34 (dd, J = 6.8, 2 Hz, 2H), 7.24 (d, J = 8 Hz, 1H), 7.04 (m, 1H), 7.0 (m, 1H), 6.80 (dd, J = 6.8, 2 Hz, 2H), 6.17 (s, 1H), 6.10 (d, J = 15.6 Hz, 1H), 4.2 (t, J = 6 Hz, 2H), 3.70 (s, 3H), 3.56 (q, J = 6 Hz, 2H), 2.3 (s, 3H). HRMS Calcd for $C_{21}H_{22}N_2O_3$ (M+K): 373.13129. Found: 373. 13093.

TG6-97-1: ^{1}H NMR ($CDCl_3$ + drops of MeOH-d_4) δ 7.52 (d, J = 15.6 Hz, 1H), 7.37 (d, J = 8.8 Hz, 2H), 7.16 (dd, J = 8.8, 4 Hz, 1H), 7.15 (dd, J = 10.8, 2.4 Hz, 1H), 6.83 (m, 3H), 6.17 (s, 1H), 6.11 (d, J = 15.6 Hz, 1H), 4.23 (t, J = 6 Hz, 2H), 3.78 (s, 3H), 3.61 (q, J = 6 Hz, 2H), 2.3 (s, 3H). Anal. Calcd for $C_{21}H_{21}FN_2O_2$: C, 71.57; H, 6.01; N, 7.95. Found: C, 71.40; H, 6.16; N, 7.88.

TG4-215-1: ^{1}H NMR. δ 7.50 (d, J = 15.6 Hz, 1H), 7.51 (d, J = 8 Hz, 1H), 7.29 (d, J = 8 Hz, 1H), 7.11 (t, J = 7.6 Hz, 1H), 7.06 (d, J = 8 Hz, 1H), 6.95 (m, 1H), 6.93 (s, *1*H), 6.77 (d, J = 8.8 Hz, 1H), 6.24 (s, 1H), 6.02 (d, J = 15.6 Hz, 1H), 5.97 (s, 2H), 5.48 (t, J = 6 Hz, 1H), 4.29 (t, J = 6 Hz, 2H), 3.70 (q, J = 6.4 Hz, 2H), 2.39 (s, 3H). HRMS Calcd for $C_{21}H_{21}N_2O_3$ (M+H): 349.15467. Found: 349.15454.

TG4-292-2: ^{1}H NMR. δ 7.51 (d, J = 15.6 Hz, 1H), 7.50 (d, J = 7.6 Hz, 1H), 7.27 (d, J = 8 Hz, 1H), 7.08 (m, 2H), 6.98 (m, 2H), 6.79 (d, J = 8.4 Hz, 1H), 6. 23 (s, 1H), 6.1 (d, J = 15.2 Hz, 1H), 5.72 (t, J = 6.4 Hz, 1H), 4. 26 (t, J = 6.4 Hz, 2H), 4.08 (q, J = 7.2 Hz, 2H), 3.83 (s, 3H), 3.6 (q, J = 6.4 Hz, 2H), 2.38 (s, 3H), 1.45 (t, J = 7.2 Hz, 3H). HRMS Calcd for $C_{23}H_{26}N_2O_3$ (M+K): 417.15750. Found: 417.15684.

TG6-109-2: ^{1}H NMR. δ 7.58 (d, J = 15.6 Hz, 1H), 7.51 (d, J = 7.2 Hz, 1H), 7.35 (d, J = 8 Hz, 2H), 7.28 (d, J = 8 Hz, 1H), 7.11 (m, 3H), 7.06 (m, 1H), 6. 23 (s, 1H), 6.19 (d, J = 15.6 Hz, 1H), 5.84 (t, J = 6 Hz, 1H), 4. 24 (t, J = 6 Hz, 2H), 3.6 (q, J = 6.4 Hz, 2H), 2.47 (d, J = 7.6 Hz, 2H), 2.38 (s, 3H), 0.9 (d, J = 6.4 Hz, 6H). Anal. Calcd for $C_{24}H_{28}N_2O$: C, 79.96; H, 7.83; N, 7.77. Found: C, 79.59; H, 7.69; N, 7.67.

TG6-94-2: ^{1}H NMR. δ 7.5 (d, J = 8.4 Hz, 1H), 7.46 (d, J = 15.6 Hz, 1H), 7.22 (m, *2*H), 7.10 (m, 4H), 6. 2 (s, 1H), 6.09 (d, J = 15.6 Hz, 1H), 5.72 (t, J = 5.6 Hz, 1H), 4. 27 (t, J = 6.4 Hz, 2H), 3.65 (q, J = 6 Hz, 2H), 2.3 (s, 3H). Anal. Calcd for $C_{20}H_{18}F_2N_2O$: C, 70.58; H, 5.33; N, 8.23. Found: C, 70.45; N, 5.39; N, 8.21.

TG6-97-2: ^{1}H NMR ($CDCl_3$ + drops of MeOH-d_4) δ 7.42 (d, J = 15.6 Hz, 1H), 7.25 (m, *2*H), 7.10 (m, 4H), 6.79 (m, 1H), 6.16 (d, J = 15.6 Hz, 1H), 6.14 (s, 1H), 4. 2 (t, J = 6 Hz, 2H), 3.57 (q, J = 6 Hz, 2H), 2.33 (s, 3H). Anal. Calcd for $C_{20}H_{17}F_3N_2O$: C, 67.03; H, 4.78; N, 7.82. Found: C, 66.81, H, 4.58; N, 7.82.

TG6-94-3: ^{1}H NMR. δ 7.49 (d, J = 7.2 Hz, 1H), 7.37 (d, J = 15.6 Hz, 1H), 7.24 (d, J = 8 Hz, 1H), 7.08 (m, *2*H), 7.02 (m, 2H), 6. 23 (s, 1H), 6.06 (d, J = 15.6 Hz, 1H), 5.56 (t, J = 4 Hz, 1H), 4. 24 (t, J = 6 Hz, 2H), 3.62 (q, J = 6 Hz, 2H), 2.37 (s, 3H). HRMS Calcd for $C_{20}H_{17}F_3N_2O$ (M+K): 397.09246. Found 397.09258.

TG6-97-3: ^{1}H NMR. δ 7.41 (d, J = 15.6 Hz, 1H), 7.15 (m, *2*H), 7.03 (m, 4H), 6.82 (m, 1H), 6.19 (s, 1H), 6.12 (d, J = 15.6 Hz, 1H), 5.78 (t, J = 5.6 Hz, 1H), 4. 25 (t, J = 6 Hz, 2H), 3.63 (q, J = 6 Hz, 2H), 2.37 (s, 3H). Anal. Calcd for $C_{20}H_{16}F_4N_2O$: C, 63.83; H, 4.29; N, 7.44. Found: C, 63.76; H, 4.13; N, 7.39.

TG4-292-1: ^{1}H NMR. δ 7.48 (d, J = 7.6 Hz, 1H), 7.40 (d, J = 15.6 Hz, 1H), 7.24 (m, 2H), 7.02 (m, 2H), 6.86 (d, J = 2 Hz, 1H), 6. 22 (s, 1H), 6.13 (d, J = 15.6 Hz, 1H), 4. 26 (t, J = 6.4 Hz, 2H), 3.8 (s, 3H), 3.63 (q, J = 6.4 Hz, 2H), 2.3 (s, 3H). HRMS Calcd for $C_{22}H_{23}BrN_2O_3$ (M+K): 481.05263. Found: 481.05200.

TG4-294-1: ^{1}H NMR. δ 7.50 (d, J = 15.6 Hz, 1H), 7.47 (d, J = 2.4 Hz, 1H), 7.27 (dd, J = 8.6, 1.6 Hz, 1H), 7.17 (dd, J = 8.8, 4.4 Hz, 1H), 7.14 (dd, J = 9.6, 2.4 Hz, 1H), 6.87 (d, J = 8.4 Hz, 1H), 6.83 (t x d, J = 8.8, 2.4 Hz, 1H), 6. 19 (s, 1H), 6.10 (d, J = 16 Hz, 1H), 5. 68 (t, J = 5.6 Hz, 1H), 4. 25 (t, J = 6.4 Hz, 2H), 3.89 (s, 3H), 3.64 (q, J = 6.4 Hz, 2H), 2.37 (s, 3H). Anal. Calcd for $C_{21}H_{20}ClFN_2O_2$: C, 65.20; H, 5.21; N, 7.24; Found: C, 64.94; H, 5.17; N, 7.12.

TG4-294-2: ^{1}H NMR. δ 7.46 (m, *2*H), 7.42 (d, J = 16 Hz, 1H), 7.26 (m, 2H), 7.05 (m, 2H), 6.85 (d, J = 8.4 Hz, 1H), 6.43 (t, J = 6.4 Hz, 1H), 6. 2 (s, 1H), 6.10 (d, J = 15.6 Hz, 1H), 4. 23 (t, J = 6.4 Hz, 2H), 3.86 (s, 3H), 3.61 (q, J = 6.4 Hz, 2H), 2.34 (s, 3H). Anal. Calcd for $C_{21}H_{21}ClN_2O_2$: C, 68.38; H, 5.74; N, 7.59; Found: C, 67.72; H, 5.76; N, 7.49.

TG6-110: ^{1}H NMR. δ 7.75 (d, J = 15.6 Hz, 1H), 7. 53 (s, 1H), 7.48 (d, J = 7.6 Hz, 1H), 7.27 (d, J = 8 Hz, 1H), 7.07 (m, 2H), 6.36 (m, 1H), 6.21 (s, 1H), 6. 19 (d, J = 15.6 Hz, 1H), 4. 23 (t, J = 6.4 Hz, 2H), 3.87 (s, 3H), 3.79 (s, 3H), 3.60 (q, J = 6 Hz, 2H), 2.37 (s, 3H). Anal. Calcd for $C_{22}H_{23}BrN_2O_3$: C, 59.60; H, 5.23; N, 6.32; Found: C, 59.47; H, 5.35; N, 6.32.

1. Jiang J, et al. (2010) Neuroprotection by selective allosteric potentiators of the EP2 prostaglandin receptor. *Proc Natl Acad Sci USA* 107:2307–2312.
2. Hagmann WK (2008) The many roles for fluorine in medicinal chemistry. *J Med Chem* 51:4359–4369.
3. Racine RJ (1972) Modification of seizure activity by electrical stimulation. II. Motor seizure. *Electroencephalogr Clin Neurophysiol* 32:281–294.
4. Borges K, et al. (2003) Neuronal and glial pathological changes during epileptogenesis in the mouse pilocarpine model. *Exp Neurol* 182:21–34.
5. Schauwecker PE, Steward O (1997) Genetic determinants of susceptibility to excitotoxic cell death: Implications for gene targeting approaches. *Proc Natl Acad Sci USA* 94:4103–4108.
6. Serrano GE, et al. (2011) Ablation of cyclooxygenase-2 in forebrain neurons is neuroprotective and dampens brain inflammation after status epilepticus. *J Neurosci* 31:14850–14860.

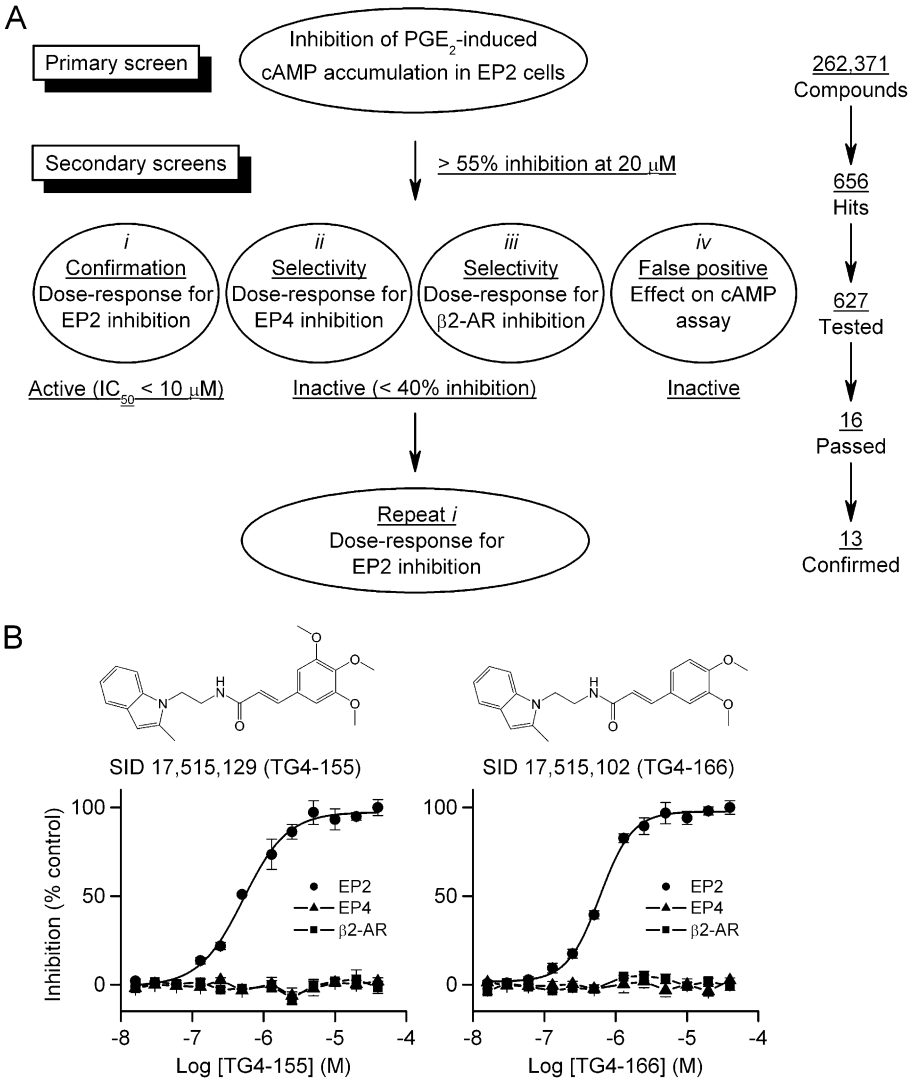

Fig. S1. High-throughput screening (HTS) and hit confirmation strategy. (*A*) Screening of a library of 262,371 compounds in 1,536-well plates yielded 656 primary hits, each of which displayed at least 55% inhibition of 1 μM PGE_2-induced cAMP accumulation in C6G-EP2 cells at 20 μM and was not inherently fluorescent at the wavelength used. Positive hits from the primary assay were tested in four secondary assays in triplicate. A compound passes assay *i* if in 8–12 point dose–response studies it shows IC_{50} < 10 μM in PGE_2 (1 μM)-induced cAMP accumulation in C6G-EP2 cells; it passes assays *ii* and *iii* if it causes <40% inhibition of PGE_2 (1 μM)- or isoproterenol (1 μM)-induced cAMP accumulation in HEK-EP4- or C6G-β2-adrenergic receptor-overexpressing cells, respectively, at the highest concentration tested (40 μM); and it passes assay *iv* if at 40 μM it does not raise the TR-FRET signal in a cell-free system in the presence of 1 μM cAMP. Each compound surviving assays *i–iv* was tested for an additional assay (*i*) and finally 13 compounds passed all tests. (*B*) Confirmed hits illustrated by SID 17,515,129 (resynthesized as TG4-155) and SID 17,515,102 (TG4-166) showed robust inhibition of PGE_2 (1 μM)-induced cAMP accumulation in C6G-EP2 cells (IC_{50} = 0.21 and 0.67 μM, respectively), without affecting prostaglandin EP4 and β2-adrenergic receptors. Data were normalized as percentage of maximum response; points represent mean ± SEM (*n* = 3).

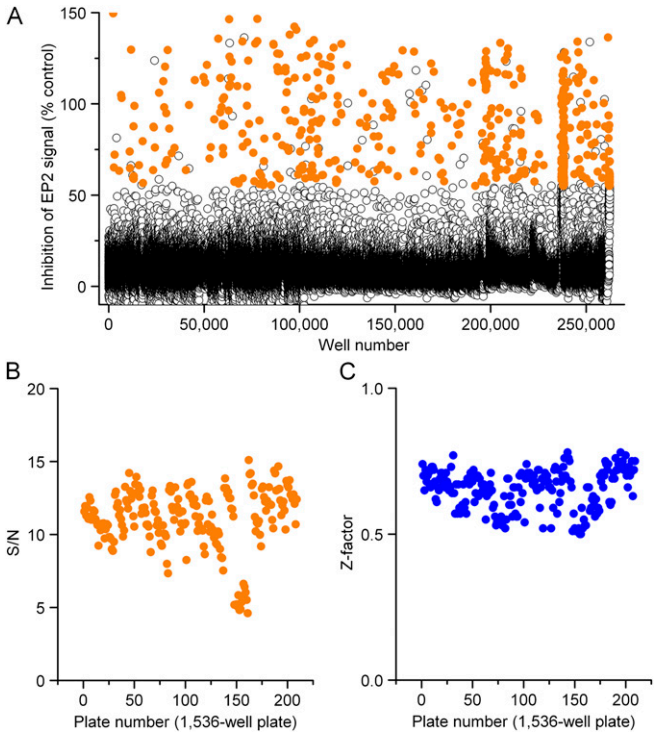

Fig. S2. Raw data from the primary screen of 262,371 compounds. (*A*) Each compound was tested at 20 μM and >55% inhibition of 1 μM PGE_2-induced cAMP accumulation in C6G-EP2 cells was considered positive. Compounds that inhibit the TR-FRET cAMP signal but are also fluorescent at 20 μM are marked as open circles. (*B* and *C*) Two measures of assay robustness, signal-to-noise ratio (*S*/N) and *Z*-factor, were used as quality control checks of the assay for screening. These two parameters were adequate for HTS (*S*/*N* > 4.5, *Z*-factor > 0.5) over the entire primary screening. $S/N = \mu/\sigma$; $Z\text{-factor} = 1 - 3 \times (\sigma_{positive} + \sigma_{negative})/|\mu_{positive} - \mu_{negative}|$; μ, mean; σ, SD.

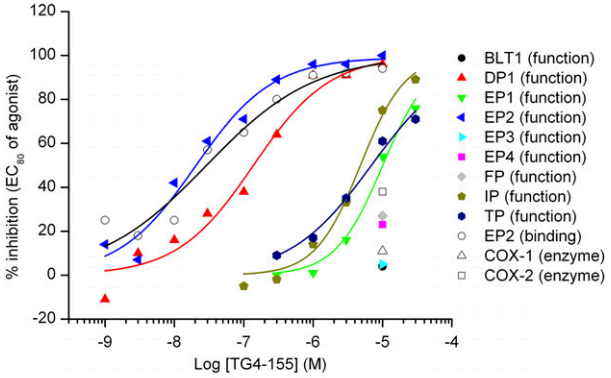

Receptor or enzyme	Antagonist activity IC_{50} (nM)	Binding assay K_i (nM)
Human BLT1	> 10,000 (*n* = 2)	
Human DP1	140	
Human EP1	10,000 (*n* = 2)	
Human EP2	20	15
Human EP3	> 10,000 (*n* = 2)	
Human EP4	> 10,000 (*n* = 2)	
Human FP	> 10,000 (*n* = 2)	
Human IP	4,800	
Human TP	6,900	
Human COX-1	> 10,000 (*n* = 2)	
Human COX-2	> 10,000 (*n* = 2)	

Fig. S3. Pharmacological activities in relevant recombinant systems. Inhibitory activities of TG4-155 were tested in cellular functional assays for a panel of recombinant human receptors: BLT1, DP1, EP1, EP2, EP3, EP4, FP, IP, and TP; radioligand binding assay for human EP2 receptor; and enzyme assays for human COX-1 and COX-2. The inhibition of DP1, EP2, IP, and TP was determined in nine-point concentration–response curves in duplicate (*n* = 2 except where unspecified).

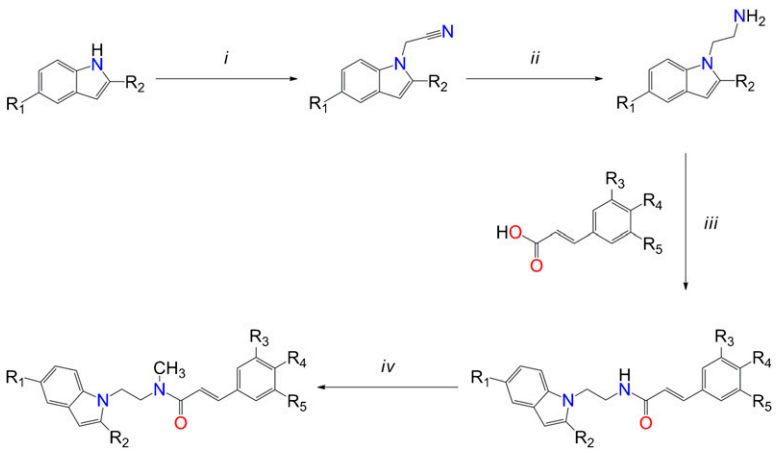

Fig. S4. Synthesis of compounds for structure–activity relationship (SAR) study. Reagents and conditions: (*i*) NaH, 2-bromoacetonitrile, *N*,*N*-dimethylformamide (DMF), room temperature (50–60%); (*ii*) lithium aluminum hydride (LAH), tetrahydrofuran (THF), 0 °C, reflux (65–70%); (*iii*) 1-ethyl-3-(3-dimethylaminopropyl)-carbodiimide hydrochloride (EDCI), dimethylaminopyridine (DMAP), CH_2Cl_2, (75–85%); (*iv*) NaH, CH_3I, DMSO (80%).

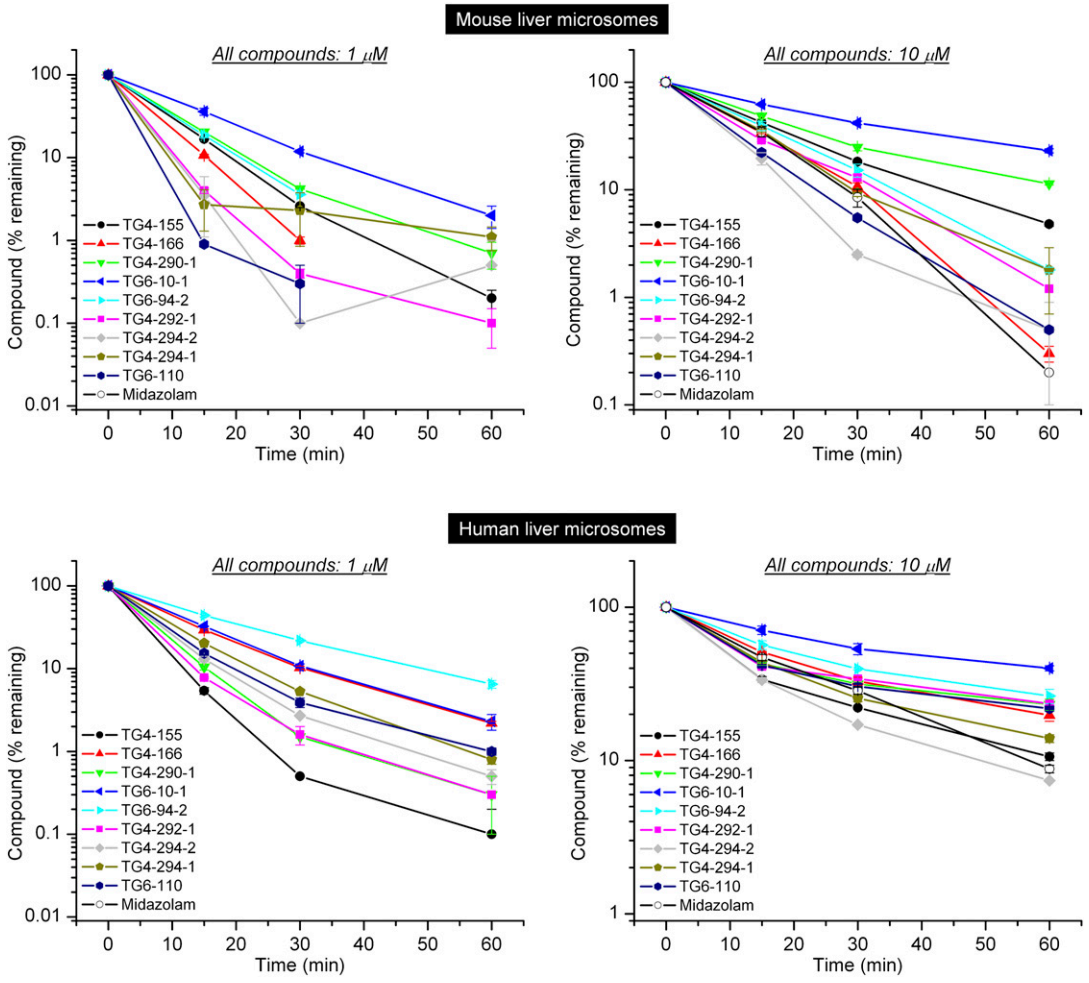

Fig. S5. Metabolic stability study in liver microsomes. Nine compounds were tested for metabolic stability at 1 μM (*Left*) or 10 μM (*Right*) in pooled mouse (*Upper*) or human (*Lower*) liver microsomes with midazolam as a control. Data are shown as mean ± SEM (n = 3).

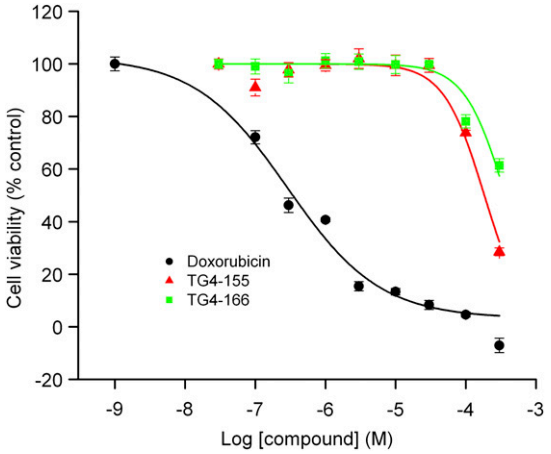

Fig. S6. Cytotoxicity of the compounds. Cytotoxicity of the test compounds was assessed in C6G cells with the CellTiter-Glo luminescent cell viability assay. All test compounds showed no significant cytotoxicity as illustrated by TG4-155 and TG4-166. TG4-155, CC_{50} = 172 μM; TG4-166, CC_{50} = 397 μM; doxorubicin as positive control, CC_{50} = 0.2 μM. Data are shown as mean ± SEM (n = 4).

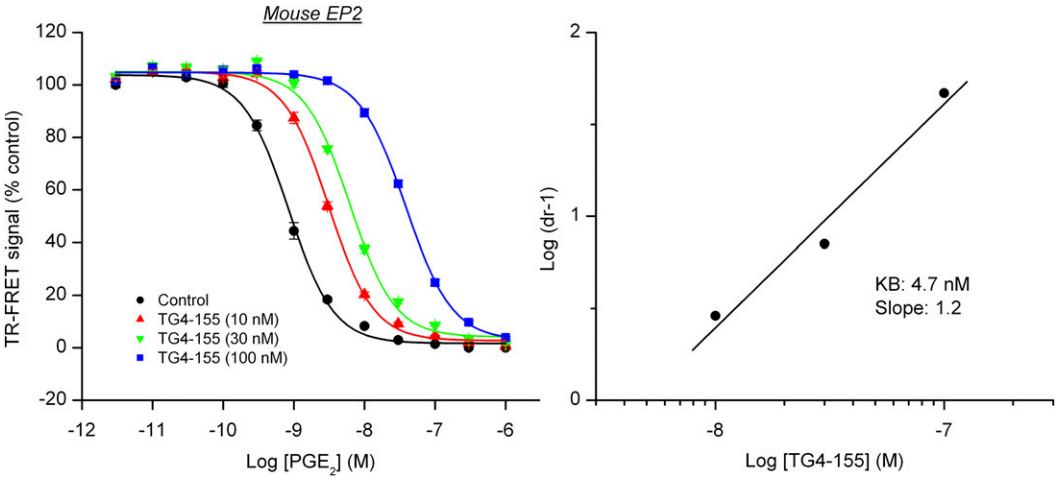

Fig. S7. TG4-155 showed high potency on mouse EP2 receptor. Schild regression analysis was performed to evaluate the inhibitory activity of the compound TG4-155 on mouse EP2 receptor in C6G-mEP2 cells. K_B = 4.7 nM; slope, 1.2. Data were normalized as percentage of maximum response; points represent mean ± SEM (n = 4).

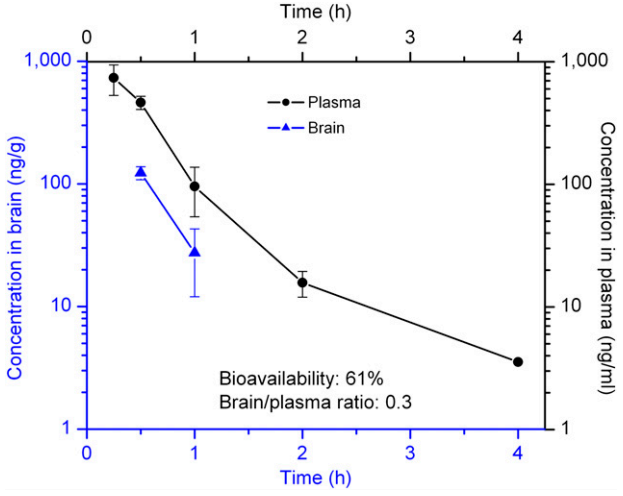

Fig. S8. Pharmacokinetic study. TG4-155 was administered to mice (3 mg/kg, i.p.). Concentrations of TG4-155 in plasma and brain were measured at different time points. TG4-155 displayed a bioavailability of 61% (i.p. route compared with i.v.), a plasma half-life ($t_{1/2}$) of 0.6 h, and a brain/plasma ratio of 0.3. Data are shown as mean ± SEM (n = 3).

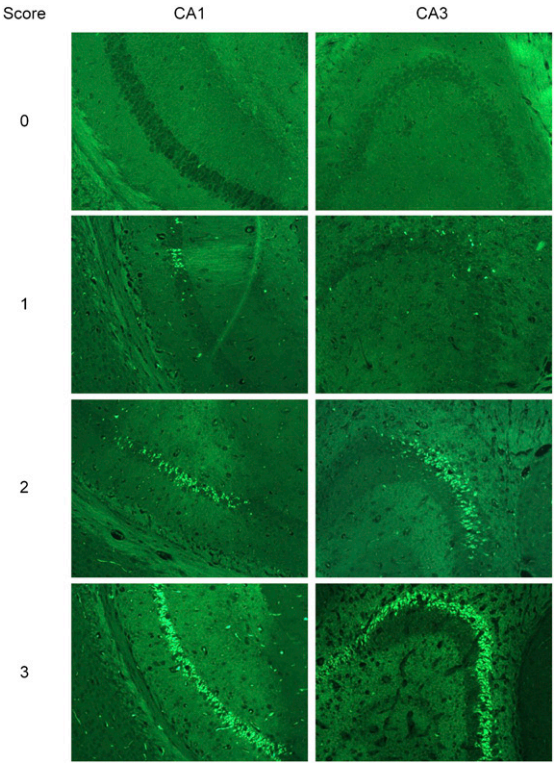

Fig. S9. Scoring criteria of Fluoro-Jade staining in hippocampal subregions CA1 and CA3. 0, <3 Fluoro-Jade–positive cells per section; 1, 3–30 cells; 2, 31–100 cells; 3, extensive Fluoro-Jade staining.